NBSIR 81-2279

Alkali Vapor Transport in Coal Conversion and Combustion Systems

J. W. Hastie, E. R. Plante, and D. W. Bonnell

High Temperature Processes Group
Chemical Stability and Corrosion Division
Center for Materials Science
U.S. Department of Commerce
National Bureau of Standards
Washington, DC 20234

May 1981

Interim Report

U.S. DEPARTMENT OF COMMERCE
NATIONAL BUREAU OF STANDARDS

NBSIR 81-2279

ALKALI VAPOR TRANSPORT IN COAL CONVERSION AND COMBUSTION SYSTEMS

J. W. Hastie, E. R. Plante, and D. W. Bonnell

High Temperature Processes Group
Chemical Stability and Corrosion Division
Center for Materials Science
U.S. Department of Commerce
National Bureau of Standards
Washington, DC 20234

May 1981

Interim Report

U.S. DEPARTMENT OF COMMERCE, Malcolm Baldrige, *Secretary*
NATIONAL BUREAU OF STANDARDS, Ernest Ambler, *Director*

Table of Contents

		Page
1.	Introduction	1
2.	Combustion Systems of Interest	4
3.	Coal Mineral Characteristics	4
4.	Corrosion by Alkalies	6
5.	Alkali Vapor Transport Modeling	8
6.	Experimental Methods	9
	6.1 The Transpiration Reactor	9
	6.2 Partial Pressure Determination	10
7.	Single Component Systems	11
	7.1 $NaCl(\ell)$ and $Na_2SO_4(\ell)$ Vaporization	11
	7.2 $K_2SO_4(\ell)$ Vaporization	13
	7.3 $KOH(\ell)$ and $KCl(\ell)$ Vaporization	14
8.	Coal Mineral Systems	15
	8.1 Alkali Benzoate/Carbonate Vaporization	15
	8.2 Illite Vaporization	16
9.	The Soda-Lime-Silica System	17
	9.1 Background	17
	9.2 KMS Measurements	18
	9.3 TMS Measurements	19
	9.4 Na_2CO_3 in Glass	20
10.	Complex Oxide Systems and Slags	21
	10.1 Background	21
	10.2 K_2O-Al_2O_3-SiO_2 System	26
	10.3 K_2O-CaO-Al_2O_3-SiO_2 System (Simplified "Western" Slag)	27
	10.4 K_2O-CaO-MgO-Al_2O_3-Fe_2O_3-SiO_2 System (Synthetic MHD Channel Slags of "Eastern" and "Western" Coal Types)	27
	10.5 Real MHD Channel Slag (K_1)	29
	10.6 Synthetic Low Melting Slag (K_2)	32
	10.7 Application of Vaporization Data to Seed-Slag Interaction	33
	10.8 Salt-Slag Alkali Exchange	35

11. Heterogeneous Reactive Gas Systems 36
11.1 Background 36
11.2 Na_2SO_4-NaOH-H_2O System 37
11.3 Illite-H_2O-H_2 System 37
11.4 Synthetic Slag (K_2)-H_2O-H_2 System 39
11.5 Glass-Combustion Gas System 42
12. Summary 45
13. Acknowledgments 45
14. References 46
15. Figure Captions 51
16. Figures 54

Alkali Vapor Transport in Coal Conversion and Combustion Systems

J. W. Hastie, E. R. Plante and D. W. Bonnell
Center for Materials Science
National Bureau of Standards
Washington, D.C. 20234

ABSTRACT

Alkali metal-containing vapor species are ubiquitous in coal conversion and combustion systems. These species originate from coal mineral and atmospheric impurities (organic and inorganic) and from ceramic construction materials. Alternatively, they are present as additives, such as with potassium seeding for MHD or with bulk glass as a particle absorbing medium, or with dolomite in fluidized bed systems. Alkali vapor transport over representative slag, glass, and simple halide, hydroxide, and sulfate systems is discussed in relation to materials and process limitations in coal-supported energy systems. Problems associated with molecular-level vapor transport measurements are also considered.

Key words: Alkali species; coal conversion; combustion; glass; mass spectrometry; slag; thermodynamics; vaporization.

1. Introduction

Vapors containing alkali metal species have diverse implications to high temperature processes (Stwalley and Koch, 1980). Potential new applications of alkalies in combustion systems include--their vapor phase catalytic action in smoke reduction (see Haynes et al., 1978 and the review of Hastie, 1975), their liquid phase catalysis of coal gasification (Gangwal and Truesdale, 1980), and their role as electron sources for magnetohydrodynamic (MHD) combustion systems. In most combustion systems, however, their presence is undesirable. This is particularly true in fossil energy systems.

More efficient coal utilization can be realized with combined power plant cycles. For instance, the post combustion gases of a conventional combustor or an advanced MHD system can be further utilized to drive a gas or steam turbine. However, the sustained durability of downstream turbine or heat exchanger components requires minimal transport of corrosive fuel impurities. Control of mineral-derived impurities is also required for environmental protection. For the special case of open cycle-coal fired MHD systems, the thermodynamic activity of potassium is much higher in the seeded combustion gas (plasma) than in common coal minerals and slags. This results in the loss of plasma seed by slag absorption and is of critical concern to the economic feasibility of MHD.

Empirical experience with conventional coal-fired power plants has indicated minerals containing alkali metal (Na, K), sulfur- and chlorine-bearing species to be the most aggressive fuel components leading to fire-side or hot corrosion (e.g., see Rapp, 1981). Species containing these elements appear to act synergistically in degrading alloy or ceramic materials. The mechanisms by which such species are released from their mineral source, transported, and deposited are not known, though the literature contains numerous speculative schemes (see Hastie, 1975, p. 216). Rational development of new control strategies, such as gas clean-up or the use of fuel additives, requires a clear understanding of the role played by the active fuel impurities. For instance, new control systems based on scavenging (e.g., absorption of alkali by glass or other oxide media) or chemical modification of the active inorganic impurities will need as design criteria information, such as species identity, concentration profiles, dew points, thermodynamic reactivity, nucleation and absorption rates and diffusivities. Such data will also be pertinent to minimization of seed-slag interaction in MHD systems.

Previous attempts to define the mode of release and transport of fuel impurities have largely been unsuccessful, owing mainly to a lack of knowledge concerning species identities. This has resulted from the inability of molecular specific measurement techniques to function under the combined aggressive conditions of high temperature, high pressure, and high chemical reactivity. We have developed several new measurement

techniques ideally suited to such conditions. The first of these techniques is a High Pressure Sampling Mass Spectrometric method for the spatial and temporal analysis of flames containing inorganic additives (Hastie, 1973; Hastie and Bonnell, 1980). The second method, known as Transpiration Mass Spectrometry (TMS) (Bonnell and Hastie, 1979), allows for the analysis of bulk heterogeneous systems over a wide range of temperature, pressure and controlled gas composition. In addition, the now classical technique of Knudsen Effusion Mass Spectrometry (KMS) has been modified to allow external control of ambient gases in the reaction cell (Plante, 1979a). Supplementary to these methods are the application, in our laboratory, of classical and novel optical spectroscopic methods for in situ measurement of temperature, flow and certain simple species concentration profiles (see Hastie and Bonnell, 1980). In combination, these measurement tools allow for a detailed fundamental examination of the vaporization and transport mechanisms of coal mineral components in a coal conversion or combustion environment.

As a long-term objective, we aim to define the mechanisms by which inorganic fuel impurities (particularly K, Na, Cl, S, and heavy metals) and additives (e.g., K in MHD) are released to or removed from the environment, transported in a gas stream and deposited in cooler or chemically less reactive regions. To meet this objective, we are addressing the following basic tasks:

(a) Measurement of species vaporization rates and related thermodynamic functions for well-characterized salt, oxide, mineral, slag, glass, and ash samples under controlled gas conditions and as a function of temperature, time, gas composition and total pressure.

(b) Development, from the basic data derived from task (a), together with auxiliary literature thermochemical data, of computer-based models for prediction of release or retention of alkali and other inorganic components under actual coal combustion, gasification, or MHD conditions.

(c) Validation of models developed from task (b) through comparisons with large-scale test data.

This paper summarizes the status of this activity. Emphasis is given to systems showing unusual behavior, or where additional lines of research are revealed. A more comprehensive presentation of data for many of the systems considered here may be found in the cited references.

2. Combustion Systems of Interest

Alkali, in the form of Na and K-containing species, can lead to a dramatic reduction in the durability of metal (alloy) and ceramic reactor components through a complex process known as hot corrosion (Rapp, ed., 1981). Examples of energy systems where this process occurs include, coal-fired utility boilers, turbines, gasifiers, MHD generators, and pressurized fluidized bed combustors (PFBC). In such cases, the alkali enters the vapor phase by vaporization from coal minerals, dolomite (Yannopoulos et al., 1977) or limestone, as in sulfur-scrubbing processes, or from air-ingested salt particles (e.g., in marine environments). Hardesty and Pohl (1979) have recently reviewed the major problem areas and data limitations relating to the properties of coal mineral matter and ash.

Even a minor amount of alkali vapor transport can be significant, as revealed by the turbine tolerance level of 0.02 ppm alkali needed for corrosion control in pressurized fluidized bed combustors (Spacil and Luthra, 1979). If we consider only the alkali halide content of the dolomite component, this tolerance level would require an alkali-scrubbing efficiency of better than 99.9999 percent for PFBC. Even if corrosion (alkali) resistant materials were available, uncontrolled alkali vapor transport would still lead to unmanageable deposits on cool downstream components. For instance, under typical coal gasifier conditions, a species partial pressure as low as 10^{-6} atm would lead to vapor transport and deposition in metric ton quantities on an annual basis.

The need for a basic understanding of alkali vapor transport in fossil energy systems can be appreciated when we consider the diversity of conditions such as temperature, pressure, chemical composition, and time scale, present in existing and developing fossil fuel technologies. Table 1 summarizes some typical process conditions.

3. Coal Mineral Characteristics

Typically, coal contains about 10 wt.% mineral matter. There is a recognized need for improved understanding of coal mineral transformations and slag-forming processes (Kolodney et al., 1976). The chemical form of alkali and halogen in coal is of considerable importance to

Table 1

Typical Coal-Conversion and Combustion Systems

Process	Temperature K	Pressure atm[e]	Comments
	Conventional Steam Plants		
	1000-1500	1	
	Pressurized Fluidized Bed Combustion		
	1200	1-10	2 % excess O_2, 300 ppm SO_2
	Coal Gasification[a,b,c]		
Cogas	570-2250	3-6	entrained/slag
Koppers-Totzek[d]	1750-2100	0	entrained/slag, medium btu
Bi-gas	1200-1920	66-100	entrained/slag
Atgas	480-1750	0-0.3	molten iron
Kellogg	1100-1480	27-80	molten salt
CO_2 Acceptor	1100-1370	10-20	fluidized (dolomite)
Hygas	920-1300	66-100	fluidized, high btu, high S
Synthane	370-1260	33-66	entrained/fluidized, high btu
Lurgi	870-1260	20-33	fixed bed, low btu
	Magnetohydrodynamics		
Open cycle-- hot walls	1500-3000	1-10	1 % K seed, fuel rich or stoichiometric

[a] Comparable conditions exist in ammonia plant secondary reformers, e.g., 1060K, 13 to 20 atm, 28 percent H_2, 50 percent H_2O, 6.4 percent CO, and 4 percent CO_2.
[b] After Crowley (1975).
[c] For technological status, see Vorres (1980) and Lenzer and Laurendeau (1976).
[d] In commercial operation.
[e] 1 atm = 1.01325×10^2 kpascal.

the mode of alkali vapor transport. Analyses of Gluskoter and Ruch (1971) suggest that halogen is present in two forms, NaCl and organic. Also, most of the potassium is present in a halogen-free highly bound form, such as for the mineral illite, or other potassium alumino-silicates. A number of coal combustion systems utilize limestone and dolomite additions for sulfur removal. These materials provide an additional source of alkali. Alkali (Na + K) contents of 0.05 to 1 wt.% are usual and the predominant mineral form is the chloride (Shearer et al., 1979).

Laboratory simulation of coal combustion indicates several modes of mineral decomposition (Sarofim et al., 1977). Submicron-size particles tend to be derived from vaporization with subsequent homogeneous and heterogeneous condensation. These particles are rich in silica (SiO vapor transport) but with large enhancements of trace metals, including alkalies, Cd, As, and other heavy metals. Various mechanisms have been suggested concerning the combustion history of the alkali components (Boow, 1972). The principal alternatives are, that NaCl is vaporized during combustion and is not incorporated into silicate minerals--at least in the initial combustion phase--or, that NaCl reacts with the ash thereby lowering the alkali activity and hence the extent of vapor phase alkali transport. This latter statement remains qualitative pending the determination of alkali activities for coal minerals and slags in combustion atmospheres.

4. Corrosion by Alkalies

Alkali vapor transport and deposition is a well-known, though poorly understood, factor in the corrosion or fouling of alloys and ceramics, both in established and developing technologies. Problem areas include oil-fired glass melting operations (Pressley, 1970), blast furnaces, boilers, turbines, coal gasification (Raymon and Sadler, 1976), MHD (Anthony, 1976; Bowen, 1979; Schneider et al., 1980) and coal-fired pressurized fluidized beds (CFCC Development Program, 1978).

In general, the corrosive effects of alkali deposits result from the high solubility of ceramic and oxide coatings (e.g., for alloys) in molten alkali sulfate, carbonate, chloride, or vanadate deposits. This solubility results from the high stability of Na (or K)-Al-silicates, or similar oxide phases. Formation of these silicates, for instance, leads

to a volume increase and loss of structural integrity in ceramic materials, e.g., see Clews et al. (1940) and Rigby and Hutton (1962). In alloy systems fluxing can also occur and this results in greatly increased oxidation rates (Rapp, ed., 1981). Even when hot corrosion is not a problem, alkali deposits can lead to fouling and thermal barrier effects. For instance, in secondary naphtha reformers, oxide deposits containing Na_2O (21 wt.%), K_2O (3 wt.%), plus SiO_2, Al_2O_3 and CaO, lead to fouling of waste heat boiler tubes (Venable, 1969).

Alkali vapor transport and deposition places severe limitations on ceramic materials for MHD generator walls and electrodes. Here, the corrosive action of K_2SO_4 and K_2CO_3-containing liquids appears to be the major problem. In the combined presence of potassium seed and coal slag, the rate of electrochemical corrosion of MHD ceramic electrodes increases by two to three orders of magnitude. Alloy corrosion at intermediate temperatures (900 to 1200 K) also can be related to formation of a liquid Na_2SO_4 phase, which prevents formation of a protective Cr_2O_3 scale and greatly enhances corrosion of Co- and Ni-Cr alloys (Luthra and Shores, 1980).

The thermodynamics of corrosive alkali salt-oxide interaction is not well established. In an assessment of research needs for materials in coal conversion, the need for carbonate-silicate melt studies, including activity and phase equilibrium measurements, was stressed (Staehle, ed., 1974). The lack of thermodynamic data for fused salts, and their reactions with oxides and alloys leading to models of hot corrosion, was also indicated.

Hot corrosion of Ni-base turbine alloys by Na_2SO_4 and K_2SO_4 is strongly dependent on the Na_2O activity in the salt (see, Huang et al., 1979; and cited work). Further activity measurements of this type are needed over a wider range of conditions. Raymon and Sadler (1976) have reviewed evidence for reactions involving alkali vapors and refractory lining materials for coal gasifiers. They indicate a pressing need for studies of alkali attack in reducing atmospheres at pressures up to 30 atm and temperatures to 1500 K.

5. Alkali Vapor Transport Modeling

Despite the incomplete state of a thermodynamic data base and limited mechanistic insight, several attempts to model alkali vapor transport in reactive atmospheres have been made. The increased sophistication of modeling efforts in recent years is demonstrated by the following examples:

(a) Coal gasification (Wilson and Redifer, 1974).

(b) Glass furnace corrosion (Kirkbride, 1979).

(c) Pressurized fluidized bed combustion (Spacil and Luthra, 1980).

In example (a), the gas composition was modeled assuming ideal solution phases and neglecting known complex vapor species, such as K_2SO_4, K_2CO_3 and alkali chlorides. These serious limitations resulted from the non-availability of oxide solution-activity data, accurate vapor species thermodynamic functions, and the inability of existing computer codes to handle non-ideal solution multiphase, multicomponent equilibrium computations.

The more recent work of example (b) modeled Na vapor transport by including NaOH, NaCl and Na_2SO_4 as vapor species, with the major uncertainties arising from neglect of solution non-ideality and inaccurate thermodynamic functions for Na_2SO_4 (see Bonnell and Hastie, 1979).

In example (c), many of the limitations represented by (a) and (b) were resolved; the greatest uncertainty resulted from the highly approximate nature of the alkali-silicate activity data (see also, comments in Section 10.1). For this system, the data base requirements are more critical since, in pressurized fluidized bed combustion, the alkali tolerance levels for downstream turbine operation are of the order of 0.02 ppm. Spacil and Luthra (1980) compared their thermochemical predictions with observed combustion gas stream alkali concentrations. Here, Na_2SO_4, NaCl, NaOH, and the K-analogues were included as significant molecular species in the thermochemical model data base. Albite and sanidine were assumed to represent the coal ash alkali-getter substrates. Fair, but encouraging, agreement between calculated and observed gas phase alkali concentration was obtained.

6. Experimental Methods

The primary experimental methods used in this study are the Knudsen Effusion Mass Spectrometric (KMS) and Transpiration Mass Spectrometric (TMS) methods, as described elsewhere (KMS, Plante, 1979a; TMS, Bonnell and Hastie, 1979). Both are modulated molecular beam methods with phase sensitive detection, and they allow for accurate measurement of both gaseous and condensible species. The basic differences between the KMS and TMS methods are, the upper pressure limits of 10^{-4} and one atm, respectively, and the upper limit gas residence times of about 0.04 and 20 sec, respectively. Thus, the TMS method will more closely approach the equilibrium condition for systems exhibiting non-equilibrium behavior. As the TMS method is still relatively novel, a brief description is given here.

6.1 The Transpiration Reactor

The TMS facility consists of a transpiration reactor mounted in one of two available multichambered (two or four), differentially pumped, vacuum ystems with a quadrupole mass filter (cross-beam) located in the high vacuum stage. Essential features of the reactor include: a sample container or boat, a boat carrier, a thermocouple for temperature measurement, a carrier gas inlet system, and a gas extraction system or probe, as shown in figure 1. The boat carrier allows for boat removal from the reactor without need for a complete disassembling of the transpiration system. Molecular beam sonic probes are typically conical nozzles with design details determined by reasonably well established gas dynamic criteria. However, for highly reactive systems, we also found it desirable to develop a more robust capillary probe, at the possible expense of sampling fidelity. For the present study, all of these components were fabricated from platinum metal. The reactor is usually operated at total pressures of 0.2 to 1.0 atm, using N_2 or Ar as a carrier gas and temperatures up to about 1700 K.

6.2 Partial Pressure Determination

For the KMS method, conversion of mass spectral ion intensities to species partial pressures is made through the basic relationships,

$$P_i = k_i I_i^+ T \quad , \tag{1}$$

and

$$k_i = \frac{GA_i(2\pi R/M_i)^{\frac{1}{2}} m_i}{ac \sum I_i^+ \, t(T)^{\frac{1}{2}}} \tag{2}$$

where, for species i; P_i is partial pressure, I_i^+ the corresponding ion intensity, T the temperature, k_i an instrument and system sensitivity constant, G a gravimetric factor, A_i an isotope abundance factor, R the gas constant, m_i the weight loss, t the time, c the Clausing factor, a the orifice area, and m_i the molecular weight (or an average value for Knudsen effusion), as described elsewhere (Plante, 1979a). In some cases, k_i for different species, but arising from the same experimental configuration, can be inter-related through known ionization cross sections, σ_i, and transmission/detector efficiencies, S_i, i.e.,

$$k_i \propto (\sigma_i \cdot S_i \cdot A_i)^{-1} \quad , \tag{3}$$

as discussed elsewhere (Bonnell and Hastie, 1979). The degree of agreement for the k_i's obtained from weight loss [expression (2)] or cross section data [expression (3)] provides a useful check on the internal consistency of the partial pressure data.

Relation (1) can also be applied to TMS data. The sensitivity factor k_i is obtained by several independent methods, thereby providing a good test of internal consistency in the data. The basic relationships are,

$$k_i = A_i \, R \, \frac{n}{V} \, \Delta t / \sum I_i^+ t \quad , \tag{4}$$

and

$$k_i = k_j \left(\frac{\sigma_j}{\sigma_i}\right)\left(\frac{S_j}{S_i}\right)\left(\frac{\bar{S}}{\bar{S}}\right)^{-1}, \tag{5}$$

where, for species i and transport gas j (N_2 or Ar); n is the number of moles of substrate transported, V the volume of gas transported, Δt the transport time interval, and $\bar{S}$ an instrument gas scattering correction ($\bar{S}$ = 0.6 to 1.0; Bonnell and Hastie, 1979). The reference or transport gas sensitivity factor k_j is readily obtained from equation (1), since the pressure of transport gas is known from an external manometric determination.

7. Single Component Systems

In complex combustion systems, alkali vapor transport can occur as the metal or as molecular species, such as NaCl, $(NaCl)_2$, NaOH, $(NaOH)_2$, Na_2SO_4, $NaSO_x$ (x = 2,3), $NaPO_x$ (x = 2,3) and, possibly, other yet-to-be established postulated species, such as Na_2CO_3 and $NaCl \cdot 2H_2O$. Potassium-containing systems show an analogous behavior. Species identities, and their basic thermodynamic functions, are usually best established by vaporization studies over the single component systems. Considerable uncertainty and literature disagreement has existed for most alkali containing systems. We have obtained new thermodynamic vaporization data for the most important systems in this category.

7.1 NaCl(ℓ) and Na_2SO_4(ℓ) Vaporization

These systems are the best established and they serve, primarily, as test cases for the TMS method. The principal TMS results for liquid NaCl may be summarized as follows. Additional detail may be found elsewhere (Bonnell and Hastie, 1979). For the reaction,

$$NaCl(\ell) = NaCl(g)$$

$$\log P_{NaCl}\ (atm) = 4.85\ (\pm\ 0.3) - 8820\ (\pm\ 200)/T\ ,$$

$$\Delta H_v\ (1300) = 40.4 \pm 0.9\ (42.7 \pm 3.5)\ kcal/mol,\ and$$

$$\Delta S_v\ (1300) = 22.2 \pm 1.4\ (24.2 \pm 0.5)\ cal/deg\ mol\ ,$$

where T is in Kelvin. These second-law data compare favorably with the JANAF (1971) evaluation of previous literature data, indicated in parentheses. Our second-law data, obtained by both TMS and KMS, for the dimerization reaction,

$$2NaCl(g) = (NaCl)_2(g) \quad ,$$

give

$$- \Delta H_d \ (1300) = 46.4 \pm 0.7 \ (47.1 \pm 3.5) \text{ kcal/mol, and}$$

$$- \Delta S_d \ (1300) = 30.2 \pm 0.6 \ (29.7 \pm 1.0) \text{ cal/deg mol} \quad ,$$

which compare favorably with the JANAF (1971) values, indicated in parentheses. Thus, the vaporization data for this system are well established.

The $Na_2SO_4(\ell)$ system has historically been difficult to characterize, due largely to containment problems. However, from our TMS and KMS second-law data (see Bonnell and Hastie, 1979), and other recent literature results, a quantitative thermodynamic description of this system is now possible. For the major vaporization process,

$$Na_2SO_4(\ell) = 2Na + SO_2 + O_2 \quad ,$$

$$\Delta H_v \ (1550) = 69.8 \pm 3 \ (71.7 \pm 0.6) \text{ kcal/mol, and}$$

$$\Delta S_v \ (1550) = 27.8 \pm 3 \ (29.7) \text{ cal/deg mol} \quad ,$$

with the JANAF (1971) data given in parentheses. For the secondary reaction,

$$Na_2SO_4(\ell) = Na_2SO_4(g) \quad ,$$

our data are consistent with those of Kohl et al. (1975), who give,

ΔH_v (1267) = 65.9 ± 3 kcal/mol, and

ΔS_v (1267) = 22.3 ± 2.8 cal/deg mol .

7.2 K_2SO_4 Vaporization

Potassium sulfate is a potentially important constituent in coal burning systems, being formed by reaction of ash/slag potassium with combustion SO_2. The solubility of K_2SO_4 (and Na_2SO_4) in coal ash is small, but reaction can occur to form K_2O (and Na_2O) dissolved in the ash with release of SO_2 and O_2. However, the deposition of K_2SO_4 (and Na_2SO_4) in hot corrosion processes indicates that K_2O (and Na_2O) is only partially removed by interaction with coal ash. This could result from slow kinetic processes, competitive chemical reactions, transport of the sulfate as gaseous molecules, or by a series of chemical reactions involving alkali-containing gaseous molecules which lead to a net transport of K_2SO_4 (or Na_2SO_4) across a temperature/concentration gradient.

The thermodynamics of K_2SO_4 and Na_2SO_4 condensed phases are generally considered to be well known and are tabulated by JANAF (1971). Thermodynamic data for the gaseous molecules are much less certain, however.

Using separate gravimetric Knudsen effusion and KMS techniques, we have obtained data for the heat of vaporization to form $K_2SO_4(g)$, and detailed results will appear elsewhere (Plante et al., 1981). From thermal data, the dissociation pressure, as represented by the reaction,

$$K_2SO_4(s,\ell) = 2K(g) + SO_2(g) + O_2(g) \quad , \qquad [1]$$

can be readily calculated. The only other reaction of comparable importance is that of the sublimation or vaporization process;

$$K_2SO_4(s,\ell) = K_2SO_4(g) \quad . \qquad [2]$$

A number of alternative vaporization processes have previously been suggested for K_2SO_4. However, one or more of the postulated reaction products [$K_2O(\ell,g)$, $SO_3(g)$] have a sufficiently positive free energy of

formation so that the proposed alternate reaction paths lead to an insignificant partial pressure of evaporation products compared to reactions [1] and [2]. Most of the previous K_2SO_4 vaporization measurements are thought to be in error because of container material reactions or, possibly, creep of liquid K_2SO_4 from the metal container (usually a platinum metal).

In the present study, weight loss measurements of $K_2SO_4(\ell)$ were made using a thermobalance equipped with a Pt Knudsen cell. Combining these data with the known dissociation pressures for reaction [1] leads to partial pressure data for reaction [2], as shown in figure 2. Complementary KMS data were also obtained. For comparison we have also indicated, in figure 2, smoothed data extrapolated from the torsion effusion measurements of Lau, et al. (1979), and data from two mass effusion measurements made by Efimova and Gorokhov (1979). The absolute pressure data from these three independent recent investigations is in unusually good agreement, but some significant differences still exist (see Plante et al. 1981). These pressure data are about 400 percent greater than the corresponding values of Ficalora et al. (1968).

7.3 KOH(ℓ) and KCl(ℓ) Vaporization

The thermodynamic stability of KOH in the vapor phase can be obtained from the Second and Third Law analyses of KOH(ℓ) vaporization as the thermodynamic functions for the liquid phase are reasonably well established. JANAF (1971) has evaluated the various disparate sets of KOH vaporization data but with considerable uncertainty. Much of the difficulty associated with obtaining reliable thermodynamic data for this system arises from its reactivity with container materials, the presence of carbonate impurity, and the coexistence of dimers and monomers. Previous studies have also been hampered by decomposition to K and H_2O. In the present work, using the TMS technique, we have suppressed this decomposition by addition of H_2O to the carrier gas.

We have obtained extensive data for the KOH(ℓ) and KCl(ℓ) systems, which will be presented in a formal publication elsewhere (Hastie et al., 1981). Representative data for KOH(ℓ) are presented here in comparison with other recent results not considered by JANAF (1971). Species partial pressure data are summarized in figure 3. Note that the

KOH species data are in good agreement with JANAF (1971), as might be expected. However, there is no agreement between workers regarding the $(KOH)_2$ species, except that the relative amounts of dimer to monomer found in the present study agree quite well with the KMS results of Gusarov and Gorokhov (1968). When the monomer and dimer partial pressures are summed, the total pressures are about a factor of two greater than the JANAF (1971) data.

With regard to the KCl(ℓ) system, the KCl species data were found to be in good agreement with JANAF (1971). However, the dimer species $(KCl)_2$ was found to have an appreciably greater enthalpy of formation than the JANAF (1971) value.

8. Coal Mineral Systems

8.1 Alkali Benzoate/Carbonate Vaporization

Part of the alkali content in coal is organically bound and the benzoate salts, NaCOOØ and KCOOØ, have been selected to model alkali release from such a state e.g., see Stewart et al. (1980). For Na and K in coal, typical organic/inorganic distribution ratios lie in the range 2 to 9, and 0.02 to 0.1, respectively. Using the TMS approach, we have obtained comprehensive data on the mechanism of Na and K release from their benzoates and the related carbonate-char systems. The detailed results will be reported elsewhere (Chakrabarti et al., 1981).

The principal findings are as follows. On heating to ∿ 800 K, sodium and potassium benzoates decompose to yield a carbonate plus char residue. At temperatures of ∿ 1000 K, this residue reacts to yield Na in the vapor phase according to the reaction,

$$Na_2CO_3(c) + 2C(c) = 2Na + 3CO \quad ,$$

and similarly for potassium. Comparison of species partial pressures with those of multicomponent equilibrium calculations indicate that this reaction is at, or near, equilibrium, a surprising result for what is formally considered a solid-solid interaction at these relatively low temperatures. Thus, the organic alkali components of coal can be a

significant source of alkali in the gas phase. Future studies are planned in the presence of reactive combustion gases, e.g., SO_2, H_2O, CO_2, H_2, and HCl.

8.2 Illite Vaporization

The clay mineral illite is frequently found as a mineral constituent of coal and is considered a major source of potassium vapor species in combustion systems. A "Beaver's Bend illite" sample was used (provided by the Morgantown Energy Technology Center) with the following composition for the major components, in wt.%: Al_2O_3(26.0), Fe_2O_3(4.4), SiO_2(60.2), K_2O(7.4), Na_2O(0.2), MgO(2.1), and S(0.1). A water analysis, carried out by heating to 1300 K in air, indicated a water content of 7.3 percent. It should be noted that water is present in the illite structure as OH groups and can be expelled only by heating to relatively high temperatures.

The melting behavior of dehydrated illite can be expected to be similar to that for an approximately 30-60-10 wt.% composition in the Al_2O_3-SiO_2-K_2O ternary system where melting begins at about 1300 K. From this analogy we can assume that over the temperature range of the present experiments (~ 1540 to 1950 K), illite (dehydrated) will be present as a reasonably homogeneous liquid.

During the initial heating period, significant release of Na and K to the vapor phase was noted over the temperature interval 1300 K to 1500 K. The predominant vapor species were SO_2 (~ 10^{-3} atm), Na (~ 10^{-6} atm), K (~ 10^{-6} atm), and possibly NaOH (~ 10^{-6} atm). The mass spectral signals for the latter species were less certain, being detected as signal/noise ratios of about two. These initial data also tended to show time dependence in the form of pressure bursts and isothermal signal decay indicative of sample inhomogeneity. Also during this initial period, the O_2 pressures were in excess of the reaction [3] level owing to reduction of Fe_2O_3 to Fe_3O_4.

Following this initial vaporization phase the principal reactions were,

$$K_2O\ (soln.) = 2K(g) + 1/2\ O_2(g) \quad , \qquad [3]$$

and

$$SiO_2 \text{ (soln.)} = SiO(g) + 1/2\ O_2(g) \quad . \qquad [4]$$

At the higher temperatures, Fe_3O_4 contributed to a small partial pressure of Fe(g), of a magnitude similar to the SiO(g) pressure. Representative vaporization data, obtained using the KMS and TMS methods, are given in figure 4 (see also table 2 in Section 10). A more detailed account of this study is given elsewhere (Hastie et al., 1979). Not all the O_2 pressure data points appear in the figure for reasons of clarity. The O_2/K pressure ratios varied from about 2 to 1/2 during the experiment. This behavior is not consistent with the vaporization stoichiometry indicated by reactions [3] and [4]. Since the K pressure is about 25 times greater than for SiO, reaction [4] is a negligible source of O_2, and most of the O_2 should result from K_2O decomposition according to reaction [3]. For this to be true, the O_2 pressure should be only about 1/4 of the K pressure and have the same temperature dependence as K. The variation of O_2/K pressure with time may be due to excess O_2 dissolved in the illite or, more likely, to iron oxide decomposition. This time-dependent oxygen activity could also account for the K pressure differences between the KMS and TMS methods, as shown in figure 4.

9. The Soda-Lime-Silica System

9.1 Background

A commercially common soda-lime-silica glass has been considered as an absorbing medium for removing fly ash particulates in combustion gas streams (Gatti et al., 1980). However, a possible limitation with this application is the release of alkali from the glass into the gas stream. Glass also has some common features with coal slag, and the basic thermodynamic data derived from glass-combustion gas studies will benefit our basic understanding of slag-gas interactions.

Description of alkali release, or retention, by glass requires accurate Na_2O activity data at various temperatures and glass compositions. However, thermodynamic activity data for glass systems are surprisingly sparse. No critical analysis, for instance of the type represented by

JANAF Thermochemical Tables (JANAF, 1971), has been made on the available data. Glass activity data for a common system can vary by several orders of magnitude, or more, depending on the measurement method used.

In the present study, we have utilized the KMS and TMS methods to obtain vaporization and activity data for a glass of initial composition (wt.%): Na_2O(17), CaO(12), and SiO_2(71) (Hastie et al., 1980a). The sample, obtained from the Ceramic, Glass and Solid State Science Division (NBS), was prepared by melting together the appropriate mixture of Na_2CO_3, $CaCO_3$, and SiO_2 in a platinum container in air to about 1800 K until all visible CO_2 was expelled, except for a residual Na_2CO_3 impurity level as discussed below. This glass is similar to those suggested as being useful for removing fly ash particulate matter from fluidized bed coal combustion systems. In addition, the binary silicate system (no CaO present) is one that has been extensively studied by a variety of methods and reliable Na_2O activity data is available [e.g., see Sanders and Haller, 1979]. There is also limited information on the effect of CaO additions on the Na_2O activity (Neudorf and Elliott, 1980). Thus, indirect comparisons can be made with activity data for the ternary system.

9.2 KMS Measurements

Partial pressures for Na and O_2 were obtained under vacuum vaporization conditions using the KMS technique. Following an initial heating period, these pressures followed the stoichiometry of the reaction,

$$Na_2O\ (soln.) = 2Na(g) + 1/2\ O_2(g)\ . \qquad [5]$$

During the initial heating period, an excessive amount of Na, as well as CO_2, was observed. Initially the CO_2 pressures approximated those for O_2 but decreased to a negligible level ($CO_2/O_2 < 0.1$) in subsequent experimental runs. Two processes appeared to be controlling the release of CO_2,

$$Na_2CO_3\ (soln.) = 2Na + 1/2\ O_2 + CO_2 \quad \text{and} \qquad [6]$$

$$Na_2CO_3\ (soln.) = Na_2O\ (soln.) + CO_2\ , \qquad [7]$$

with the former predominating in the early and lower temperature phase of the experimental runs, and the latter at higher temperatures and later observation times.

Figure 5 summarizes Na partial pressure curves for two experimental runs. Experimental details have been presented elsewhere (Hastie et al., 1980a) and the data points closely followed the curves given in figure 5. The vertical bar represents the maximum conceivable error that could have arisen with the KMS (run 1) data. Several data sets from the literature are indicated for comparison. Neudorf and Elliott (1980) measured Na_2O activities in the binary silicate solution, as well as the effects of CaO on the Na_2O activity, using an emf method. We have extrapolated their data to our experimental conditions based on the effects of Na_2O and CaO content on the Na_2O activity. The data point of Cable and Chaudhry (1975) was obtained by a classical transpiration method under conditions where surface segregation effects were negligible. Similarly, the data point of Sanders et al. (1976) represents a stirred-melt transpiration experiment where surface depletion is also unlikely. The curve of Argent et al. (1980) represents Knudsen effusion mass spectrometric data (without beam modulation).

9.3 TMS Measurements

Glass vaporization in a N_2 atmosphere was monitored using the TMS technique. Representative Na-partial pressure curves are given in figure 5. Note that these partial pressures are more than an order of magnitude greater than those obtained by the KMS technique. Ideally, both sets of data should coincide. We believe that the explanation for this apparent discrepancy is as follows.

Under the conditions of the KMS experiments, the rate of alkali removal was about an order of magnitude greater than for TMS. This may be seen by the calculated composition change in the respective glass samples, i.e., KMS(3) final wt.% Na_2O = 13.3 and TMS(2) = 16.9 as compared with the initial composition of 17.0 wt.%. During the initial phase of each type of experiment, excessive amounts of CO_2 and Na were released. Only when about one percent of the glass Na_2O was depleted did the excess CO_2 and Na become negligible in the KMS experiments. As this level of alkali depletion was never reached during the TMS experiments,

we believe that these latter data correspond to the anomalously high Na pressures found in the early phase of the KMS experiments. These high alkali pressures can be attributed to the presence of unreacted Na_2CO_3 impurity in the original glass samples, even though care was taken to avoid this in the glass preparation. Residual carbonate impurity is a common problem with glass experimentation e.g., see Cable and Chaudhry (1975).

We calculate from the time-integrated CO_2 and excess Na signals that the initial concentration of impurity Na_2CO_3 was 0.45 wt.%. From the relative amounts of Na, O_2, and CO_2 released prior to vaporization from the silicate itself, two types of impurity-related vaporization processes appear to be present, as represented by reactions [6] and [7]. Comparison of the TMS and KMS data indicates that the activity of Na_2O (solution), produced by reaction [7], is substantially greater than that for the silicate-bound Na_2O characteristic of the pristine glass. Apparently, the Na_2O produced in situ by carbonate decomposition is not readily incorporated into the silicate matrix, at least on the time scale of the vaporization measurements. Formally, we can consider Na_2CO_3 as a solute, in a metastable glass solution, and with an activity defined by reaction [6], as discussed in the following Section (9.4). Alternatively, one could argue that under the higher vaporization rate conditions typical of KMS, surface depletion of alkali led to the relatively low Na-pressures observed, e.g., see Cable and Chaudhry (1975). However, no significant isothermal time dependent vaporization was noted on the several minute time scale of individual KMS measurements. Also, the KMS(1) pressures are greater than the stirred-melt data of Sanders et al., (1976) which would not be the case in a surface-alkali depleted system.

9.4 Na_2CO_3 in Glass

We have interpreted the anomalously high alkali vapor pressures of the TMS experiments described in Section 9.3 in terms of impurity Na_2CO_3 decomposition in a glass solution. By monitoring the release of CO_2, and integrating over time, we have determined the mole fractions of Na_2CO_3 present at the various measurement temperatures and times. Hence, from the observed partial pressures for reaction [6], and the

corresponding reference state values (JANAF, 1971), we can calculate Na_2CO_3 activity coefficient data, as shown in figure 6. These data appear to be thermodynamically reasonable and tend to support the alkali carbonate impurity interpretation of alkali vaporization differences between the KMS and TMS experiments (see Section 9.3). We can likewise argue that the data of Cable and Chaudhry (1975), shown in figure 5, also appear to suffer from this impurity problem, even though they also took precautions to eliminate residual carbonate during the glass synthesis process.

Future studies should be pursued under controlled doping conditions and in atmospheres containing CO_2 and O_2. The known synergistic effect of CO_2 on O_2-solubility in silicate melts at very high gas pressures has, in fact, been interpreted in terms of Na_2CO_3 formation in solution. Effects of this type could significantly enhance alkali vapor transport in practical combustion systems.

10. Complex Oxide Systems and Slags

10.1 Background

As part of a program of systematic studies on potassium-containing slag systems, vaporization data have been obtained for a series of synthetic-binary, ternary, quarternary and sexternary oxide mixtures, as well as an actual MHD coal-slag sample. Virtually no experimental thermodynamic activity data exist for these systems. Even for the most studied relatively simple K_2O-SiO_2 system, existing data is extremely crude and incomplete. Comparison of our activity data for this system with those reported by Charles (1967), as based on the moist-atmosphere transpiration data of Preston and Turner (1933), indicate several order-of-magnitude differences, with the Charles's results being low. Likewise, the estimates of Spacil and Luthra (1980), as based on the phase diagram, yield activities one to two orders of magnitude lower than our experimental values (for details, see CFCC, 1978).

Table 2 contains a summary of selected potassium vaporization data for these systems. With a few noted exceptions, the oxygen partial pressures coupled stoichiometrically with potassium, in keeping with reaction [3]. Hence, $K_2O(\ell)$ activities can be derived, to a good to

excellent approximation, using the corresponding dissociation-pressure data for pure liquid K_2O. That is,

$$A_{K_2O} = (P_K)^{5/2}/2K_p \quad , \qquad (6)$$

where K_p is the dissociation constant (see reaction [3]) for pure liquid K_2O. We have derived a temperature dependent expression for K_p as follows. From JANAF (1971), K_p data for $K_2O(s)$ are available. Combining these results with the fusion enthalpy and entropy data of Natola and Touzain (1970), and an estimated C_p for liquid K_2O of 25 cal/deg mol, leads to the expression,

$$\log K_p\ [K_2O(\ell)] = \frac{-23751}{T} + 11.7723 \quad .$$

The potassium vapor pressure data were obtained under neutral conditions using the TMS technique. For most coal-conversion and combustion systems of interest, iron will be present in the slag as Fe_3O_4. Hence the data reported in table 2 were obtained, for the most part, at temperatures (and run times) where Fe_2O_3 (slag) had essentially converted to Fe_3O_4 (slag). Evidence of this reduction was conveniently established by monitoring the O_2-pressure. These results can also be applied to systems where O_2-sources other than reaction [3] are present. In this case, the K-pressures are converted to activities using equation (6). The activity data are then combined with the known equilibrium constants for reaction [3], and the assigned O_2-pressures, to yield the new K-pressure data. For relatively low temperature oxidizing conditions, where Fe_2O_3 (slag) may be present, we can reasonably assume that the present alkali activity data will be valid. That is, the various forms of iron oxide do not significantly affect the alkali activity.

Experimental details and an extended discussion of these potassium vapor pressure results have either appeared, or will appear, elsewhere, as indicated in table 2. In general, the potassium vaporization data followed the expected Clausius-Clapeyron behavior, as indicated in table 2. Exceptions to this behavior could be traced to:

(a) residual alkali carbonate impurities resulting either from the sample synthesis method, or from condensation out of MHD plasmas with actual slag samples;

Table 2

Summary of Alkali Vaporization Data for K-Containing Complex Oxide and Coal Slag Systems

System[a]	Phases[a,b,e]	Temperature[c] K	K-Pressure[d,e] atm A	B	Comments[e]
K_2O-SiO_2	Solution 44 to ~ 5[K_2O]	1300-1800	4.721	15624	Pressures higher than earlier data of Plante et al. (1975) because of orifice effect.
			C = 9.32		
K_2O-Al_2O_3	$KAlO_2$ → $K_2O{\cdot}5Al_2O_3$[f]	1300-1800	5.489	15036	P_K independent of bulk composition. Plante et al. (1975).
	$K_2O{\cdot}9Al_2O_3$ → Al_2O_3[f]	1500-1800	7.487	21453	
K_2O-ZrO_2	$K_4Zr_5O_{12}$-ZrO_2	1100-1450	4.524	12873	Plante (1977).[g]
K_2O-Fe_2O_3	$KFeO_2$-$K_2O{\cdot}6Fe_2O_3$[f]	1150-1450	4.524	12873	Phase boundary composition slightly dependent on T.
	$K_2O{\cdot}6Fe_2O_3$-Fe_3O_4	1200-1600	7.028	16750	Data adjusted for constant K/O_2. Plante (1979b).
K_2O-Al_2O_3-SiO_2 ($KAlSiO_4$)[h]	$KAlSiO_4$, $K_2O{\cdot}9Al_2O_3$, $KAlSi_2O_6$	1400-1650	8.722	20923	Probably not equilibrated because of slow condensed phase kinetics. Plante (1979c, 1980a)
K_2O-Al_2O_3-SiO_2[h]	Possibly $KAlSi_2O_6$, Al_2O_3, $K_2O{\cdot}9Al_2O_3$ ~ 22[K_2O]	1600-1900	7.068	20763	Evidence of melt formation.
	Phases uncertain ~ 17[K_2O]	1600-2000	6.350	20693	
	Phases uncertain ~ 11.5[K_2O]	1750-2150	4.667	19800	
	Liquid + $3Al_2O_3{\cdot}2SiO_2$ (10.8[K_2O]) (mullite)	1800-2150	4.464	20424	Decreasing T-chronology used to minimize composition change.

System[a]	Phases[a,b,e]	Temperature[c] K	K-Pressure[d,e] atm		Comments[e]
			A	B	
Simplified Western Slags K_2O-CaO-Al_2O_3-SiO_2	Solution + $KAlSiO_4$ at higher K_2O content	1400-1900	5.228 C = 7.887 exp-2, D = 1.741 exp-3, E = 1.825 exp-2	16794	Composition range, [K_2O] 3-14, [CaO] 17-36, [Al_2O_3] 14-36, [SiO_2]-balance. Standard dev. ~ 30 percent, maximum dev. ~ 100 percent. Additional data for 20[K_2O] compositions have been obtained. Plante (1980a,b,c,d; 1981).
Real MHD Channel Slag (K_1): [K_2O] 19.5, [Al_2O_3] 12.1, [Fe_2O_3] 14.3, [CaO] 3.8, [MgO] 1.0, [SiO_2] 46.8, [Na_2O] 0.5.	$KAlSiO_4$ major + minor unidentified crystalline phase + slag	1600-1800	5.564	16650	Illinois no. 6 coal, UTSI test sample. Initially high pressure of K due to presence of K_2SO_4 and K_2CO_3 (0.2 percent S). Equation corresponds to [K_2O] ~ 14. Hastie et al. (1980).
Synthetic Western Channel slag: [K_2O] 22.7, [Al_2O_3] 24.6, [Fe_2O_3] 5.3, [CaO] 9.3, [MgO] 3.3, [SiO_2] 34.8.	$KAlSiO_4$ + glassy phase	1500-1700	6.818	18472	[K_2O] 18.9-17.6. Plante and Cook (1978).
Synthetic Eastern Channel slag: [K_2O] 23.6, [Al_2O_3] 25.5, [Fe_2O_3] 12.5, [CaO] 1.8, [MgO] 0.6, [SiO_2] 36.0.	$KAlSiO_4$ + glassy phase	1600-1750	6.831	19056	23.3-22.1 [K_2O]. Linear portion of AB, BC curves in figure 9. Plante and Cook (1978).
Illite: [K_2O] 7.4, [Al_2O_3] 26.0, [Fe_2O_3] 4.4, [MgO] 2.1, [SiO_2] 60.2.	Liquid	1550-2085	6.286	20642	Hastie et al. (1979).

System[a]	Phases[a,b,e]	Temperature[c] K	K-Pressure[d,e] atm		Comments[e]
			A	B	
Low Melting Synthetic Slag (K_2): [K_2O] 8.7, [Al_2O_3] 11.1, [Fe_2O_3] 12.0, [CaO] 13.9, [MgO] 7.9, [SiO_2] 47.3.	Liquid	1470-1820	6.231	17863	6[K_2O]. Initial $P_{O_2} \geq P_K$, but later fell to the level of K_2O (see text). Hastie et al. (1980).

[a]Initial compositions, given in weight percent (wt.%). Note, actual analyses given not normalized to 100 percent. Fe_2O_3-containing systems usually converted to Fe_3O_4 with loss of O_2 under vacuum or neutral atmosphere vaporization conditions.

[b]Phases indicated are solid.

[c]Temperature range over which experimental data were taken.

[d]Results obtained by KMS. See comments for applicable compositions. Potassium partial pressure data can be represented, to a good approximation, by the empirical form,

$$\log P \text{ (atm)} = A - B/T + C + D - E \quad ,$$

where A is an entropy term and B is enthalpy; C, D, and E are the factors by which the concentrations (normally in wt.%) of K_2O, CaO, and Al_2O_3, respectively, are to be multiplied. The factor C in the K_2O-SiO_2 system is to be multiplied by the K_2O mole fraction squared. P refers to pressure (atm) of elemental K, as the only K-species present. T is temperature in Kelvin. Other data for individual compositions may be found in the reports cited (see comments). Note, similar data-fits are obtained for compositions expressed in mole %.

[e]Square brackets indicate weight percent composition. Exp-2 denotes, for instance, 10^{-2}.

[f]Exact crystalline phase compositions uncertain.

[g]Pressure could be low by a factor of two because of vapor unsaturation (large orifice). Also, K_2CO_3 contamination present.

[h]Compositions constrained to mole ratio Al_2O_3/SiO_2 = 0.5.

(b) alkali carbonate and sulfate phases in real slag samples;
(c) non-equilibrium effects in the condensed phase;
(d) non-equilibrium between the condensed and vapor phase leading to an unsaturated vapor;
(e) changing phase boundaries due to incongruent vaporization;
(f) rapid loss of alkali pressure with time (T constant), possibly resulting from surface depletion in highly viscous systems; and,
(g) Fe-controlled redox reactions resulting in changing oxygen and, hence, K-partial pressure data with temperature and time.

A systematic study of systems with a progressive increase in the number of components was made in order to isolate and quantify such behavior. Some of these exceptional cases are discussed in the following sections.

10.2 K_2O-Al_2O_3-SiO_2 System

The K_2O-Al_2O_3-SiO_2 system has the potential for forming several stable or metastable phase assemblages in which the K_2O activity is fixed according to the phase rule (see table 2). However, in practice, we observe the K pressure (and, hence, K_2O activity) to be dependent on the bulk K_2O concentration. This effect could result from several non-equilibrium factors including, slow condensed phase kinetics attributable to the complex crystal chemistry, changing composition in the β-alumina phase (which extends from K_2O/Al_2O_3 ratios of 1/5 to 1/9), or to dissolution of SiO_2 in the β-alumina phase. The vapor pressure equation in table 2, for the three phase region, is based on the highest alkali-pressures which were effectively independent of composition.

Other evidence for non-equilibrium behavior is shown in figure 7. In the previous experimental run, alkali-pressure data were obtained as a function of increasing temperature up to 1860 K. On decreasing the temperature, lower pressures were found than for the increased-temperature run, particularly at 1760 K and below. As shown in figure 7, continuation of this experiment initially produced low pressures over the AB interval. The temperature and K_2O concentration at which this phenomenon was noted is reasonably consistent with the phase diagram which shows eutectic melting at 1829 K and 22 wt.% K_2O. (Levin et al., 1964). We attribute this loss of alkali-volatility to formation at the sample surface of a

frozen eutectic melt which is probably glassy in nature. For an equilibrium system, this melt would recrystallize but for the present experimental conditions there was probably insufficient time. The phase being depleted by vaporization is $KAlSiO_4$ (kalsilite) and the pressure-loss results from the slow alkali transfer rate across the frozen eutectic which results in partial isolation of the remaining $KAlSiO_4$. Note, in figure 7, the upward curvature of the AB interval with increasing temperature. This unusual behavior probably results from remelting of the eutectic barrier-phase with an increased rate of alkali transport through this barrier together with incorporation of additional $KAlSiO_4$ in the eutectic melt. The BC interval of figure 7 represents vaporization from this regenerated phase. This effect was noted only for experiments where a small amount of the $KAlSiO_4$ phase remained and where a potassium-deficient surface glaze acted as a diffusion barrier to vaporization. Representative vapor pressure data for "normal" behavior in this system are summarized in table 2.

10.3 K_2O-CaO-Al_2O_3-SiO_2 System (Simplified "Western" Slag)

These four component systems, designated as Simplified "Western" slags in table 2, are relatively well behaved in terms of alkali vaporization and are useful model systems for sub-bituminous basic coal slags. The data have been cast in analytical form, as summarized in table 2.

10.4 K_2O-CaO-MgO-Al_2O_3-Fe_2O_3-SiO_2 System (Synthetic MHD Channel Slags of "Eastern" and "Western" Coal Types)

Literature compositional analyses of several hundred coal ash and a few MHD channel slags, containing potassium seed, have been evaluated for the purpose of selecting representative compositions for modeling. Table 2 indicates the compositions selected as most representative of MHD channel slags of "Eastern" and "Western" coal types. These slags are non-glassy with $KAlSiO_4$ as the dominant crystalline phase (in both slag types) and small amounts of $KAlSi_2O_6$ and at least one unidentified phase (for "Eastern" slag type only). Thus, the bulk composition is not as meaningful a variable as for homogeneous glassy slags. Vapor pressure

measurements were made using a relatively small effusion orifice (0.34 mm diameter) to prevent vapor unsaturation effects found earlier on similar mixtures but with larger orifices (0.5 to 1.0 mm). Steady state pressures were not obtained until about ten percent of the K_2O content had been depleted by vaporization. Excess oxygen was vaporized during this initial experimental phase with reduction of FeO_x (x = 1.5 to 1.33). Following this initial reduction period, the oxygen partial pressures were, within experimental error, what would be expected for K_2O dissociation (reaction [3]).

Figure 8 compares vapor pressure data for "Western" and "Eastern" slags. This comparison clearly demonstrates a basic difference between these slag types in that "Eastern" slags require about twice as much K_2O-content to achieve similar alkali pressures as for "Western" slags. This effect results from the higher concentration of basic CaO and MgO in "Western" slags leading to a less complex silicate structure in the "Western" slag and, hence, a less bound form of K_2O.

The vaporization behavior of the "Eastern" slag, in the composition range 24 to 21 wt.% K_2O, is very different to that for the "Western" slag as shown in figure 9. Here, the vapor pressure curves show a significant break at location X, the position of which depends on the amount of sample vaporized. Note the significant positive deviation of the observed K and O_2-pressures (XC interval) from those obtained by extrapolating the higher temperature linear portion of the respective curves. The curves labeled AB in figure 9 were obtained prior to the curves labeled BC. At temperatures above 1620 K, these two curve sets are seen to merge into a single linear portion. This non-linear behavior is attributed to a changing oxygen potential in the slag. At the higher temperatures, the oxygen partial pressures were greater than predicted by K_2O dissociation alone (reaction [3]). However, at the lower temperatures (XC region), less oxygen was observed than expected for reaction [3]. Apparently, FeO_x undergoes reduction at temperatures above 1620 K with release of additional O_2 (above the K_2O level). Below this temperature, FeO_x is oxidized by the O_2 resulting from K_2O dissociation. It is significant that thermodynamic equilibrium is maintained during this redox process, as evidenced by a common K_2O activity over the AX and XC intervals (data not shown in fig. 9). For the lower FeO_x content "Western" slags this effect was not observed.

10.5 Real MHD Channel Slag (K_1)

Detailed TMS and KMS studies were made of vapor transport over a high liquidus temperature (~ 1700 K) potassium-enriched coal slag with initial composition as indicated in table 2. This slag sample was obtained by combustion of Illinois No. 6 coal with additional potassium added to the combustor (see Hastie et al., 1980b). Note that this slag composition lies between those of the "Eastern" and "Western" coal-types. For identification purposes, this slag is given the designation K_1. X-ray diffraction data indicated that the bulk of the slag potassium was present as the compound $KAlSiO_4$. TMS analysis indicated that about two percent of the slag potassium was present in relatively volatile form, mainly K_2SO_4 and K_2CO_3.

10.5.1 Identity of Volatile Species

The as-received potassium-enriched coal slag was subjected to a series of heating cycles (runs) in nitrogen carrier gas. During the initial heating cycle, mass spectral scans, obtained using the TMS technique, revealed many volatile species in addition to the expected K and Na species. The following species were positively identified: H_2O, CO_2, SO_2, O_2, K, and Na. Some of the other low-intensity ion signals can be very tentatively assigned to the species (some hypothetical): KO or KOH, KS or KSH, SiS, SiSH, H_2S, H_2SO_4, and KSiO. From JANAF (1971), we can expect to see KOH under these conditions. Some of these more minor species may result from slag occlusions and metastable phases and most likely do not represent an equilibrium release from the slag. Following this initial heating cycle, the only significant slag vapor species were K and O_2, and these were present in the approximate stoichiometric ratio expected for K_2O decomposition.

10.5.2 Initial Species Partial Pressure--Temperature Dependence

The initial volatiles showed a non-monotonic variation of partial pressure with temperature, as shown in figure 10. These volatiles constitute only a few percent of the total slag components and are not

representative of the bulk slag composition. However, they do provide a sufficiently high flux of alkali (Na, K) and SO_2 to be a potential source of corrosion in downstream MHD components. The high initial partial pressures of SO_2, CO_2, K, and Na are indicative of the presence of alkali sulfate and carbonate in the slag. An additional contribution to low temperature ($T < 1300$ K) alkali release could result from the high H_2O content leading to the formation of volatile hydroxide species (KOH). However, no definitive hydroxide signals were observed. (The discussion of Section 11 is pertinent in this regard.) Note that at $T > 1400$ K, the potassium pressures fall below those expected from $KAlO_2$, but that the SO_2, CO_2, and H_2O pressures are still relatively high. Apparently, at this stage, the K produced by sulfate and carbonate decomposition is retained in the bulk slag. After further heating, the sample was virtually depleted of Na, SO_2, and CO_2; H_2O also continued to fall-off in pressure to a negligible level. Following this initial clean-up period, the sample showed a more normal vaporization behavior and representative data are summarized in table 2.

10.5.3 K_2O Activity Coefficients

Most of the bulk-slag composition changes result from K_2O dissociative vaporization. Therefore, a continuous monitoring of the K-partial pressure (and O_2) allows one to calculate the slag composition at any stage of an experiment using relationships (1), (2), and (4) and the known initial sample weight and composition. For both the TMS and KMS methods, the basic experimental requirement for monitoring the bulk composition is the measurement of significant species partial pressures as a function of time during an experimental run. An independent check on this approach can be provided by chemical analysis of the sample remaining at the end of a run. In general, when all the significant species are measured and the ionization cross sections are known (though not necessary in the present case), this in situ approach to monitoring composition changes provides a good mass balance at any stage of the experiment, as was shown for the NaCl and Na_2SO_4 test systems reported elsewhere (Bonnell and Hastie, 1979).

Since the mole fraction of K_2O can be defined at any stage of an experiment, it is possible to convert K-partial pressures to K_2O activity coefficients using equation [6]. By varying the amount of K_2O present in the slag during a vaporization run, we were able to follow the dependence of the K_2O "apparent" thermodynamic activity on temperature and composition. The term "apparent" is used to emphasize that the slag system may not always be in a state of complete thermodynamic equilibrium. Typical data, expressed in activity coefficient form [$\gamma(K_2O)$], are given in figure 11. Most of these data were obtained below the liquidus temperature. Good agreement was obtained between the TMS and KMS-based data at relatively high temperatures ($\sim$ 1600 K). From this observation, we can conclude that the high temperature data represent thermodynamic equilibrium because of the greatly different residence time scales involved, i.e., TMS $\sim$ 10 sec and KMS $\sim$ 0.04 sec. The largest experimental uncertainty in comparing activity coefficient data from the two different techniques (KMS and TMS) is the accuracy of the K_2O mole fraction, which is probably uncertain by ten percent in each case. Comparison of these data with those for the K_2O-SiO_2 system, for instance, at 10 mole % K_2O in each case and 1700 K, indicates a K_1 slag activity coefficient of about 30 times that for the binary system. This observation is consistent with the more basic character of the K_1 slag.

Note in figure 11, the non-monotonic nature of the activity coefficient curves. For normal non-ideal solution behavior, we would expect a linear monotonic relationship with a negative slope representing a negative partial molar enthalpy of solution for K_2O in the slag. This type of behavior occurs for segments of each run (see fig. 11), e.g., for run 1, up to about 1430 K, and for run 2 between 1430 and 1630 K. However, the run 1 data are anomalous as they were obtained during the initial heating period when K_2SO_4 and K_2CO_3 decomposition was a significant source of additional K. The rapid reduction in $\gamma(K_2O)$ as the temperature is increased beyond 1430 K results from the virtually complete depletion of these relatively volatile forms of potassium. For runs 2 and 3, the initial reduction of $\gamma(K_2O)$ with increasing temperature is believed to be due either to diffusion limited (in solid slag) K-transport to the slag surface or to changes in the mode of O_2 release from the slag, for instance, through Fe_3O_4 dissociation. The onset of increasing $\gamma(K_2O)$

with temperature is believed to arise either from an as-yet unspecified physiochemical change in the slag, leading to a less viscous (but still solid) form and increased diffusion, or to depletion of secondary O_2 sources. At higher temperatures, the bulk composition changes rapidly (see mole fractions in fig. 11) and leads to a peaking in $\gamma(K_2O)$. We believe that the data for runs 2 and 3, at temperatures in excess of 1450 K, represent an equilibrium vaporization condition, particularly as the KMS and TMS data are in agreement for these conditions. Clearly, these unusual trends in the $\gamma(K_2O)$ data indicate the difficulty involved in making a priori predictions of real slag vaporization behavior.

10.6 Synthetic Low Melting Slag (K_2)

A lower liquidus temperature ($\sim$ 1480 K), less viscous (as compared with the K_1 sample) synthetic slag was prepared for studies analogous to those performed for the K_1 system. It was hoped that this slag would not show the same anomalous activity behavior, at lower temperatures, as for the K_1-MHD coal slag sample.

Under free vaporization (KMS) or N_2-atmosphere (TMS) conditions, the predominant vapor species in this system are K and O_2, as shown in figure 12. The initial excess of O_2 present in this slag is believed to result from the following sources. First, the preparation procedure of melting and pouring in room air may have led to oxygen absorption by the sample. Second, pressure bursts of K and O_2 (and CO_2) were noted in the initial phase of the TMS experiments and particularly near the liquidus temperature, e.g., at 1500 K in figure 12. This effect is attributed to K_2CO_3 impurity. Third, reduction of Fe_2O_3 to Fe_3O_4, with release of excess O_2, is favorable at these temperatures and, in fact, has a similar temperature dependence to that of the initial O_2 data shown in figure 12. Using the JANAF (1971) thermochemical data for Fe_3O_4 and Fe_2O_3, it is possible to predict O_2 partial pressures for given condensed phase activities. On this basis, the initial experimental data of figure 12 at 1600 K, for instance, are consistent with $\sim$ 50 percent and 25 percent Fe_2O_3 reduction for the KMS and TMS experiments, respectively.

The KMS data were obtained using the integrated ion intensity-weight loss method of pressure calibration [Eq. (2)], taking into account the

additional weight loss due to Fe_2O_3 reduction. Calibration of the TMS data, on the other hand, was made using the relative ionization cross section approach [Eq. (3)]. The apparent difference between the KMS and TMS data, indicated in figure 12, is related to the problem of additional sources of O_2 already mentioned. That is, the TMS data were obtained at an earlier stage of the sample history, where the high O_2 pressure depresses the K-pressure by the mass-action effect. In fact, if the data are converted to K_2O activities, the KMS and TMS data are in satisfactory agreement. Such agreement is good evidence of system thermodynamic equilibrium. At a later phase of the KMS experiments, the O_2/K pressures were of the correct stoichiometry for $K_2O(\ell)$ decomposition.

A second type of time dependent phenomenon was observed for this slag using the TMS method, as shown in figure 13. Once an isothermal condition was achieved, the K-pressure decreased with time. This result could be taken as evidence of surface depletion of K (and O_2) from the sample, due to the bulk diffusion rate being too small relative to the surface vaporization rate. Also, this effect was found to be much less pronounced at higher temperatures where the diffusion rates are higher. However, this initial interpretation (Hastie et al., 1980b) no longer seems reasonable. The order-of-magnitude greater vapor transport rates for KMS vs TMS experiments would indicate lower apparent activities in the former case due to surface depletion effects. However, in practice the KMS activities are somewhat higher. Hence, this time dependent phenomenon is attributed to the combined effects of K_2CO_3 impurity decomposition, as noted previously for the analogous glass system in Section 9, and, to FeO_x reduction, as noted with the "Eastern" slag data in figure 9. That this latter effect was more apparent in the TMS, versus the KMS, experiments can be attributed to the much higher transport rates and shorter FeO_x reduction times for the latter case.

10.7 Application of Vaporization Data to Seed-Slag Interaction

A key factor for successful MHD operation is the degree of interaction between plasma potassium seed and the slag medium. Using slag activity data from the present studies, it is possible to predict conditions under which plasma seed will be continuously depleted by slag

absorption of alkali. Plante et al. (1975) presented similar arguments earlier, based on their data for the binary oxide systems. A more definitive analysis can now be made from the present data on complex synthetic and actual slag systems.

The stability of K_2O in slag solutions can be readily determined by comparison of the K_2O dissociation pressure-product ($P_K^2 \cdot P_{O_2}^{\frac{1}{2}}$) data in the slag phase with that in the plasma phase, as represented in figure 14. This dissociation pressure (DP) expression is a convenient representation of slag activity data [activity = DP, soln./DP, $K_2O(\ell)$]. The DP curves for the plasma phase were calculated using a multicomponent equilibrium computer program, assuming stoichiometric combustion of $CH_{0.7}$ with air (4/1 mole ratio N_2/O_2) and KOH, K, KO, K^+, and e as vapor phase species. Pressures of ten and one atmosphere were chosen to be representative of the MHD combustor and the channel-diffuser-downstream seed recovery units, respectively. Corresponding curves for the actual MHD slag (K_1) and the Synthetic "Western" and Simplified "Western" slags, were calculated from the experimental vapor pressure data given in table 2.

Comparison of the DP curves for plasma and slag indicate temperatures for K_2O slag saturation in the range of 2100 to 2300 K at 10 atm, and 1850 to 2050 K at one atm, depending on the slag type and composition. The approximately 200 K equivalence temperature difference between actual and model slags is attributed, primarily, to the low CaO concentration in the former case. Slag absorption of K_2O at the channel and diffuser surfaces depends strongly on the plasma-surface interface temperature. Experimentally, these interface temperatures are difficult to measure though the data reported by Self (1979) indicate that they are in the region of 2100 to 2300 K. At these temperatures, and at atmospheric pressure, slags with at least 18 wt.% K_2O are predicted to be stable with respect to the plasma phase, as indicated in figure 14. Such a prediction is in accord with the observed 19.5 wt.% K_2O content of the actual MHD slag (K_1). Conceivably, calculations of this type, together with actual slag analyses, could be used to infer the actual interface temperatures.

Note that the DP equivalence temperatures in figure 14 are significantly lower for the atmospheric conditions characteristic of downstream units. Also, as the temperature decreases, the slag dissociation pressure-product decreases much faster than for the plasma, resulting in a supersaturated alkali vapor concentration at the plasma-slag interface. Hence, additional K_2O will be absorbed by the slag. Below the dewpoint, this seed will tend to deposit on the slag surface in a relatively non-bound form, such as the alkali sulfate or carbonate, which is desirable from a seed-recovery point of view. As the temperature decreases, the reduced slag species diffusion rates and the increased tendency for phase separation to occur will allow K_2SO_4 and K_2CO_3 deposits to remain at, or near, the slag surface, as is found in practice. Indirect evidence of this type of deposition may be seen in figure 10.

10.8 Salt-Slag Alkali Exchange

The common disposition of alkali in coal minerals is Na as NaCl and K as K_2O--bound in a low-activity silicate phase. Thus, during coal conversion, Na is expected to be released to the vapor phase more readily than K. However, the possibility of NaCl-K_2O (slag) interaction to produce KCl-Na_2O (slag) could greatly enhance K-release to the vapor phase. Also, in MHD slags, where about 20 wt.% K_2O content is possible, the problem of recovering this lost seed could likewise be resolved through replacement by NaCl. The feasibility of such an exchange process was tested by a TMS monitoring of the vapor phase over the system, NaCl + K_1 slag (19.4 wt.% K_2O). Details of this study will be given elsewhere (Hastie et al., 1981b), but the main observations are as follows.

When a thin layer of powdered NaCl was present on the surface of the K_1 slag, a rapid exchange reaction occurred near the melting point of NaCl, i.e.,

$$NaCl(\ell) + K_2O\ (slag) = KCl(\ell) + Na_2O\ (slag) \quad .$$

This result is demonstrated in figure 15, where the observed partial pressures of NaCl and KCl are expressed in thermodynamic activity form.

Note the marked decrease in NaCl activity and concomitant increase in KCl activity just above the melting point of NaCl. After a heating period of about 50 min., the NaCl sample was virtually depleted, as was the KCl product. Insufficient salt was present in the initial mixture to convert all the available K_2O to KCl. However, 90 percent of the initial NaCl was converted to Na_2O (slag) with stoichiometric release of KCl. About six percent of the available K_2O was converted to KCl vapor, and we expect that nearly complete removal of K_2O from the slag would have been possible if sufficient NaCl was present. The remaining ten percent NaCl was lost by vaporization before, and during, the exchange process. During the isothermal, constant activity, phase of the exchange process (20 to 40 min. region of fig. 15), a potassium vapor transport enhancement factor of,

$$\frac{P_{KCl}}{P_K \text{ (no NaCl)}} \sim 10^4$$

was observed. Also, during this period, the high KCl activity suggests formation of an essentially ideal solution of KCl-NaCl, as well as the establishment of thermodynamic equilibrium. Note the near unit NaCl activity in the initial phase of the experiment (fig. 15), which confirms the calibration factors used to convert mass spectral ion intensities to partial pressures and reflects establishment of thermodynamic equilibrium. Additional study of this exchange process is in progress.

11. Heterogeneous Reactive Gas Systems

11.1 Background

In the previous sections, we have considered alkali vapor transport from condensed phase systems in the absence of external influences, such as reactive gases. However, some of the component gases of combustion systems, such as H_2O, HCl, SO_2, O_2, CO, and H_2, can be expected to significantly modify alkali vapor transport through mass action effects or formation of new molecular species. Some representative cases are considered as follows.

11.2 Na_2SO_4-NaOH-H_2O System

From a thermodynamic viewpoint, H_2O should react with Na_2SO_4 to form NaOH vapor at high temperatures. However, surprisingly, on the relatively long time scale of TMS measurements, no such reaction was observed. When a small amount (0.25 to 1 percent) of condensed NaOH was mixed with the Na_2SO_4, reaction with H_2O vapor was observed. Also, the alkali vapor pressure enhancement was thermodynamically consistent with the process,

$$H_2O + Na_2SO_4(c) = 2NaOH(g) + SO_2 + 1/2\ O_2 \quad .$$

Details of this study will appear elsewhere (Bonnell et al., 1981).

11.3 Illite -H_2O-H_2 System

Vaporization of potassium from the highly acidic illite system, in neutral atmospheres, is expected to provide a relatively insignificant source of alkali in most coal combustion systems (see Section 8.2). However, in the presence of reactive combustion gases, such as H_2O and H_2, thermodynamic considerations predict a significant KOH partial pressure. In addition, an increase in the K-pressure should result from a reduction in the O_2 pressure, in the presence of H_2. However, KMS experiments did not indicate formation of KOH or additional K in the presence of H_2 gas. Thus, thermodynamic equilibrium does not appear to have been established in this heterogeneous system, even though the temperatures were sufficiently high to have normally ensured a rapid approach to equilibrium.

Further evidence of this lack of thermodynamic equilibrium was provided by monitoring formation of SiO by H_2 reduction of SiO_2, present either as the silicate in illite or as pure silica. Figure 16 shows that SiO production from both forms of SiO_2 is about one to two orders of magnitude less than the equilibrium values represented by the JANAF (1971) curve. In the absence of H_2 or H_2O, the SiO and O_2 pressures were reasonably consistent with an equilibrium system.

The kinetic limitation does not appear to result from the heterogeneous reaction process but, rather, from a lack of equilibrium for the homogeneous reaction,

$$H_2O = H_2 + 1/2\ O_2 \quad , \qquad [8]$$

as shown in figure 17. When H_2 was the added reactant, K_p for this reaction was found to be about two orders of magnitude greater than the accepted value. This discrepancy would result if a large fraction of H_2 effused through the Knudsen cell without reaction. However, when H_2O was the added reactant, K_p was also greater than the known value and by an order of magnitude. This case represents closer agreement over the system where H_2 was added. Some of this improvement may result from the lower H_2O pressures used and/or the possibility for H_2O to undergo decomposition on the effusion cell surfaces. To form H_2O, however, H_2 must undergo one or more collisions with the oxide sample surface. The points agreeing most closely with the theoretical H_2O dissociation curve in figure 17 were obtained by assuming that $P_{H_2} = 2P_{O_2}$, rather than using the measured P_{H_2} to calculate K_p. This assumption would be true for a static system in which H_2 and O_2 are formed only by decomposition of water. For Knudsen effusion, the rate of escape is inversely proportional to the molecular weight and, at steady state conditions, $P_{H_2} = 1/2\ P_{O_2}$. Under these dynamic conditions, K_p would be 1/4 the static value. Vaues of K_p calculated on the basis of this assumption are not shown in figure 17. The K_p values for the dissociation of H_2O using either of these two assumptions scatter within a factor of two around the JANAF (1971) curve over most of the temperature range. At the highest temperatures, the agreement is less satisfactory because of excess O_2 production from residual illite in the effusion cell. Values of K_p for water addition, where the observed P_{H_2} is used to calculate K_p, indicate that the mass spectrometric method is overestimating the H_2 pressure by almost an order of magnitude. This error could result from H_2O reduction on the furnace element and/or the outer surface of the Knudsen cell. However, we have observed this lack of equilibrium for the H_2O decomposition reaction in other systems and, more particularly, with the TMS method,

which has less opportunity for furnace decomposition reactions, as well as a much longer characteristic gas residence time.

If we consider the rate limiting step in the homogeneous H_2O-O_2-H_2 system as,

$$O_2 + H_2 = 2OH \quad ,$$

then the literature kinetic data (Baulch et al., 1972) indicate reaction times in the approximate range of 10 to 100 sec for our experimental conditions ($\sim$ 1600 K). Thus, the TMS residence time range of 1 to 20 sec is marginal for equilibrium in the H_2O system, and the KMS system is even less favorable (as observed experimentally). However, at temperatures in excess of 2000 K, this limiting rate is several orders of magnitude faster, and equilibrium can be attained, as noted earlier (Hastie et al. 1980b).

Evidence of non-equilibrium in H_2O-H_2-condensed phase systems was also noted recently by Sasaki and Belton (1980). They observed O_2 partial pressures one to two orders of magnitude less than the equilibrium values at a temperature of 1423 K over liquid Cu. However, in the presence of a Pt wire catalyst, they were able to closely approach equilibrium at residence times not too different from those of the present mass spectrometric studies.

11.4 Synthetic Slag (K_2) - H_2O - H_2 System

In order to extend the vapor transport conditions in slag systems to a reducing hydrous environment similar to that present in coal gasification, a series of TMS and KMS measurements were made using H_2 or H_2O as the initial reactant gas. With the TMS system, compositions of H_2-N_2-H_2O up to 10 vol % H_2 were attained prior to hydrogen-induced corrosive loss of the transpiration reactor.

11.4.1 Effect of H_2 on K-Vaporization

As H_2 was introduced to the slag system, the O_2 concentration decreased and K and H_2O increased, as expected for the process,

$$K_2O(slag) + H_2 = 2K + H_2O. \qquad [9]$$

Typical TMS data are given in figure 18 where the H_2 partial pressure was varied over the range 10^{-4} to 10^{-2} atm. Note the pronounced hysterisis effect for increased versus decreased H_2 and H_2O-content. Though not shown here, this effect is also present in the K_2O activity data, as calculated from the observed K and O_2-pressures. Hence the system is not at thermodynamic equilibrium. From the established equilibrium constants for reaction [3] with K_2O (slag) and K_2O (pure liquid), together with the measured K_2O activity data, we calculate,

$$K_p\ [9] = 209 \text{ at } 1650 \text{ K}.$$

The corresponding experimental value, obtained from the measured partial pressures of K, H_2, and H_2O, is

$$K_p\ [9], \text{ obs.} = 4.2 \text{ at } 1650 \text{ K}.$$

Thus the system is far from equilibrium.

11.4.2 Effect of H_2O on K-Vaporization

Similar TMS experiments were performed but with H_2O as the added reactant and a non-reducing atmosphere. An unexpected K-pressure dependence on H_2O was found, as shown in figure 19. No hysterisis effects were observed in this case. A similar, though less pronounced (factor of four less effect on K-pressure), H_2O-induced K vaporization effect was noted in the more acidic and more viscous MHD (K_1) slag sample (Hastie et al., 1980b).

For the H_2O-pressure and temperature conditions used, KOH should have formed according to the process,

$$K_2O\ (slag) + H_2O = 2KOH. \qquad [10]$$

However, no KOH was observed in the TMS mass spectra. We also established the K^+ precursor as atomic K, from the pure KOH data (Section 7.3) and

appearance potential measurements. A higher temperature study, using the KMS method, did show the expected formation of KOH in the presence of added H_2O. However, the KOH-pressures were about an order of magnitude below predicted equilibrium values, even though the correct H_2O pressure dependence was found, as shown in figure 20.

The apparently anomalous H_2O-induced increase in K-pressure can be explained as follows. Literature water solubility data for aluminate and silicate melts [e.g., see Schwerdtfeger and Schubert (1978)] suggest solubilities of at least several hundred ppm for our experimental conditions. Various acid-base reaction mechanisms have been suggested to explain water solubility in silicate melts, as summarized by Turkdogan (1980). For basic melts, H_2O acts as an acid and enhances the silicate network structure, and vice-versa for acid (high silica) melts. Though apparently not previously recognized, these structural changes should be reflected in the alkali activity data. Thus, we can reasonably expect an activity increase when water is incorporated into the silicate matrix of the relatively basic K_2 slag. Reaction sets of the type,

$$H_2O + O^{2-} \text{ (slag)} = 2(OH^-)$$

$$K_2O \text{ (slag)} = 2K + 1/2\ O_2, \text{ and}$$

$$O_2 + 2e = 2O^{2-},$$

would be consistent with the observed one-half power dependence of $\log P_K$ on $\log P_{H_2O}$ (see fig. 19). These structural changes should also be reflected in viscosity data. The water-solubility viscosity enhancement effects noted by Brower et al. (1980) for a similar slag are consistent with the present activity trends. For more basic systems a decreased alkali activity is possible. The recent observations of Gray (1980), where water vapor decreased alkali vaporization rates in low silica glasses, could be interpreted in this manner.

We believe that a similar water vapor solubility enhancement of alkali vapor transport is possible in soda-lime-silica glass systems, and work is in progress to verify this. Some of the disparities between

various glass vaporization studies may well result from variations in water content and, hence, alkali activities. The common explanation for water vapor enhanced alkali vapor transport over silicates has revolved around formation of volatile NaOH (Sanders and Haller, 1977) and KOH (Charles, 1967) species. However, no direct test for the presence of these species has been made, and the possibility of water vapor enhancement of atomic Na and K transport exists in these systems.

Mention should also be made of the possible effect of H_2O dissociation (i.e., reaction [8]) to yield vapor phase H_2, which was suggested by Horn et al. (1979) as a factor in ceramic degradation. However, in the present system there is an additional source of O_2 and, at thermodynamic equilibrium, K should be H_2O-independent except for the noted H_2O-solubility effect.

11.5 Glass-Combustion Gas System

Certain combustion gas components can promote alkali vapor transport in glass systems. Such transport is important in glass melting. Also, glass had been suggested as a medium for trapping particulate material in combustion gas clean-up processes, such as for pressurized fluidized bed combustion (Gatti et al., 1980).

Using our experimental activity data for Na_2O in glass (see Section 9.2), we have modeled the effect of a typical combustion gas mixture on alkali vaporization (Hastie et al., 1980a). For this purpose we have acquired, and adapted to our computers, a code known as SOLGASMIX (Eriksson, 1975) which is unique in its ability to deal with non-ideal solution multicomponent heterogeneous equilibria. Previous attempts to model this type of problem have been limited to ideal solution assumptions (Kirkbride, 1979). As is demonstrated in table 3, if solution non-ideality is neglected, drastic errors result in the prediction of alkali vapor transport processes. Table 3 and figure 21 summarize the predicted alkali species partial pressures. The thermodynamic data base was constructed mainly from the JANAF (1971) compilation. Additional details of this study will be presented elsewhere.

Table 3

Effect of Atmosphere and Solution Non-Ideality
on Alkali Vapor Species Distribution

Glass: Na_2O (17 wt.%), CaO (12 wt.%), SiO_2 (71 wt.%)

Initial Gas Composition (mole percent): H_2O (4), O_2 (5), CO_2 (12), N_2 (76), SO_2 (2), HCl (1)[d]

Temperature: 1400 K

Total Pressure: one atm

Species	Non-Ideal Soln. N_2 atm. Pressure (atm)	Ideal Soln. Gas atm.[b] Pressure (atm)	Non-Ideal Soln. Gas atm.[b] Pressure (atm)
Na	3.1(-7)[a]	2.2(-4)	1.0(-7)
NaOH	--	8.5(-2)	9.2(-5)
NaCl	--	9.8(-3)	8.8(-3)
Na_2Cl_2	--	7.1(-4)	5.8(-4)
Na_2SO_4	--	4.4(-6)	4.4(-6)
Na_2O Activity[c]	3.4(-8)	1.62(-1)	3.4(-8)
Total Na	3.1(-7)	9.6(-2)	1.1(-2)
No Halogen	3.1(-7)	8.5(-2)	1.0(-2)

[a]Computer notation, e.g., 3.1(-7) = 3.1×10^{-7}.

[b]Refers to mixed gas composition given above.

[c]Infinite supply of glass assumed and activity not affected by vaporization loss.

[d]Halogen content represents an upper limit for combustion of a high-halogen coal in a salty (marine location) atmosphere. For typical low-halogen U. S. coals, the chloride concentration would be $\sim$ 0.01 mol % and the NaCl pressures correspondingly less.

The principal results of these calculations can be summarized as follows:

(a) The presence of one percent halogen enhances alkali transport by more than two orders of magnitude at 1200 K, but only by a factor of four at 2000 K.

(b) Only in a N_2 atmosphere is atomic Na a significant vapor species.

(c) If glass is treated as an ideal solution, then halogen has only slight enhancement effect on alkali transport, i.e., NaOH is the predominant species.

(d) Glass non-ideality reduced alkali transport by an order of magnitude in the presence of halogen but by three orders of magnitude in a halogen-free reactive atmosphere.

(e) Sulfur has a much lower effect than halogen, or H_2O, on alkali transport and for the lower temperature range (< 1500 K) most of the sulfur is removed from the gas stream due to $Na_2SO_4(\ell)$ formation. Note, however, (in fig. 21) the non-monotonic production of Na_2SO_4 vapor species with temperature, leading to significant alkali vapor transport over the temperature interval 1300-2000 K.

(f) At 1200 K, alkali vapor transport covers the range of 7 to 1200 ppm, depending on the absence or presence of halogen, respectively.

From these results, it is clear that alkali release from glass under combustion gas atmospheres will be a significant source of alkali (i.e., > 10^{-6} atm) in the combustion gas stream at temperatures greater than 900 K, even for low-halogen combustion conditions. We should stress that these predictions are sensitive to the assumption that the gas stream attains thermodynamic equilibrium with the glass substrate. Our experimental data on sulfate and complex oxide systems indicates that such an equilibrium is not always readily attained. Incorporation of rate processes into heterogeneous reaction models must await further experiments to develop the necessary data base and mechanistic understanding.

12. Summary

During the past few years, substantial progress has been made in developing a thermodynamic data base and in providing mechanistic insight into the vaporization processes for alkali metal salt, oxide, silicate, and complex slag systems. Experimental techniques have been improved or newly developed suitable for thermodynamic studies of complex, corrosive alkali-containing systems, including coal slags. Computer codes are now available for thermodynamic calculations of heterogeneous non-ideal solution multicomponent equilibrium systems, such as for combustion-coal slag interactions. Vapor phase problems remaining include: (a) possible formation of novel species at very high gas pressures (10 to 100 atm); (b) lack of mechanistic understanding and rate data for non-equilibrium heterogeneous systems; (c) non-availability of computer codes for heterogeneous rate-limited systems; and (d) development of diagnostic methods and data for actual coal-conversion and combustion systems, including MHD channels, coal gasifiers, pressurized fluidized beds, and gas turbines.

13. Acknowledgments

A significant portion of this work was supported by the Department of Energy. Mr. Art Sessoms provided valuable technical assistance. Valuable discussion with our colleagues, Drs. W. Horton and L. Cook, is also acknowledged.

14. References

Anthony, A. M. (1976). Rev. Int. Hautes Temp. Refract. 13, 230.

Argent, B. B., Jones, K., and Kirkbride, B. J. (1980). "Vapors in Equilibrium with Glass Melts", in The Industrial Use of Thermochemical Data, Barry, T. I., ed., p. 379, The Chemical Society, London, UK.

Baulch, D. L., Drysdale, D. D., Horne, D. G., and Lloyd, A. C. (1972). "Evaluated Kinetic Data for High Temperature Reactions", Vol 1, Butterworths, London and Washington, DC.

Bonnell, D. W., and Hastie, J. W. (1979). "Transpiration Mass Spectrometry of High Temperature Vapors", in Characterization of High Temperature Vapors and Gases, Hastie, J. W., ed. NBS-SP 561, p. 357, US Government Printing Office.

Bonnell, D. W., Sanders, D. M., and Hastie, J. W. (1981). "Alkali Vapor Transport in the Na_2SO_4-H_2O System", to be published, (High Temperature Science).

Boow, J., (1972). Fuel, 51, 170.

Bowen, H. K. (1979). "Ceramics for Coal-Fired MHD Power Generation," in Materials Science in Energy Technology, p. 181, Academic Press, New York, NY.

Brower, W. S., Waring, J. L., and Blackburn, D. H. (1980). "Slag Characterization: Viscosity of Synthetic Coal Slag in Steam", NBSIR 80-2124.

Cable, M., and Chaudhry, M. A. (1975). Glass Tech., 16, 125.

CFCC Development Program, Combustion Chemistry Evaluation (1978). FE-2357-40. General Electric, Schenectady, NY.

Chakrabarti, A., Bonnell, D. W., Stewart, G., and Hastie, J. W. (1981). "Vaporization Studies of Alkali Benzoates in Reactive Atmospheres", to be published.

Charles, R. J. (1967). J. Amer. Ceram. Soc., 50, 631.

Clews, J. H., Richardson, H. M., and Green, A. T. (1940). Trans. Brit. Ceram. Soc., 39, 139.

Crowley, M. S. (1975). Am. Ceram. Soc. Bull., 54, 1072.

Efimova, A. G., and Gorokhov, L. N. (1979). High Temp. (English Trans.), 16, 1019.

Eriksson, G. (1975). Chemica Scripta, 8, 100.

Ficalora, P. J., Uy, O. M., Muenow, D. W., and Margrave, J. L. (1968). J. Am. Ceram. Soc., 51, 574.

Gangwal, S. K., and Truesdale, R. S. (1980). Energy Res. 4, 113.

Gatti, A., Goldstein, H. W., McCreight, L. R., and Semon, H. W. (1980). "Feasibility Study of Coal Slag Based Glasses for Hot Gas Clean-up", Report, FE-2068-32 to DOE (February).

Gluskoter, H. J., and Ruch, R. R. (1971). Fuel, 50, 65.

Gray, W. J. (1980). Radioactive Waste Management, 1, 147.

Gusarov, A. V., and Gorokhov, L. N. (1968). Russ. J. Phys. Chem. 42, 449.

Hardesty, D. R., and Pohl, J. H. (1979). "The Combustion of Pulverized Coals-An Assessment of Research Needs", ibid, Bonnell and Hastie.

Hastie, J. W. (1973). Combust. Flame, 21, 49.

Hastie, J. W. (1975). "High Temperature Vapors-Science and Technology", Academic Press, New York, NY.

Hastie, J. W., Plante, E. R., Bonnell, D. W., and Horton, W. S. (1980a). "Molecular Basis for Release of Alkali and Other Inorganic Impurities From Coal Minerals and Fly Ash", Dec. 1980 Report to DoE Morgantown, WV.

Hastie, J. W., Bonnell, D. W., Plante, E. R., and Horton, W. S. (1980b). "Vaporization and Chemical Transport Under Coal Gasification Conditions", NBSIR 80-2178.

Hastie, J. W., and Bonnell, D. W. (1980). "Molecular Chemistry of Inhibited Combustion Systems", NBSIR 80-2169.

Hastie, J. W., Plante, E. R., and Bonnell, D. W. (1979). "Molecular Basis for Release of Alkali and Other Inorganic Impurities from Coal Minerals and Fly Ash", Nov. 1979 Report to DOE, Morgantown, WV.

Hastie, J. W., Bonnell, D. W., and Zmbov, K. (1981a). "Transpiration Mass Spectrometric Analysis of KOH(ℓ) and KCl(ℓ) Vaporization", to be published.

Hastie, J. W., Plante, E. R., and Bonnell, D. W. (1981b). "Slag-Alkali Halide Exchange Reactions", to be published.

Haynes, B. S., Jander, H., and Wagner, H. G. (1978). Symp. (Int.) Combust., 17th p. 1365. The Comb. Inst. Pittsburgh, PA.

Horn, F. L., Fillo, J. A., and Powell, J. R. (1979). J. Nucl. Mater., 85, 439.

Huang, T., Gulbransen, E. A., and Meier, G. H. (1979). J. Metals, p. 28.

JANAF (1971). Joint Army, Navy, Air Force Thermochemical Tables, 2nd ed., NSRDS-NBS 37, US Government Printing Office, Washington, DC. See also later supplements for 1971-1981.

Kirkbride, B. J. (1979). Glass Tech., 20, 174.

Kohl, F. J., Stearns, C. A., and Fryburg, G. C. (1975). "Sodium Sulfate: Vaporization Thermodynamics and Role in Corrosive Flames", NASA TMX-71641.

Kolodney, M., Yernshalmi, J., Squires, A. M., and Harvey, R. D. (1976). Trans and J. Brit. Ceram. Soc. 75, 85.

Lau, K. H., Cubicciotti, D., and Hildenbrand, D. L. (1979). J. Electrochem. Soc., Solid State Science and Technology, 126, 490.

Lenzer, C. R., and Laurendeau, M. N. (1976). "Gasification of Pulverized Coal Within Swirling Flows: An Interpretive Review", The Combustion Laboratory School of Mechanical Engineering, Purdue University, West Lafayette, Indiana 47907.

Levin, E. M., Robbins, C. R., and McMurdie, H. F. (1964). Phase Diagrams for Ceramists. p. 407, Am. Ceram. Soc., Columbus, OH.

Luthra, K. L., and Shores, D. A. (1980). J. Electrochem. Soc., Solid-State Science and Technology, 127, 2202.

Natola, F., and Touzain, Ph. (1970). Can. J. Chem. 48, 1955.

Neudorf, D. A., and Elliott, J. F. (1980). Met. Trans., 11B, 607.

Plante, E. R. (1977). In, Development, Testing and Evaluation of MHD Materials, NBS Quarterly Progress Report to DOE, H. P. R. Frederikse, T. Negas, and S. J. Schneider, March.

Plante, E. R. (1979a). "Vapor Pressure Measurements of Potassium Over K_2O-SiO_2 Solutions by a Knudsen Effusion Mass Spectrometric Method", p. 265, ibid, Bonnell and Hastie.

Plante, E. R. (1979b). In Properties of Electronic Materials, NBSIR 79-1976, J. R. Manning, ed.

Plante, E. R. (1979c). In, MHD Materials-Seed/Slag Interactions and Effects, S. J. Schneider, NBS Report to DOE, December.

Plante, E. R. (1980a). In, MHD Materials-Seed/Slag Interactions and Effects, NBS Quarterly Progress Report to DOE, S. J. Schneider, March.

Plante, E. R. (1980b). In, MHD Materials-Seed/Slag Interactions and Effects, NBS Quarterly Progress Report to DOE, S. J. Schneider, June.

Plante, E. R. (1980c). In, MHD Materials-Seed/Slag Interactions and Effects, NBS Quarterly Progress Report to DOE, S. J. Schneider, September.

Plante, E. R. (1980d). In, MHD Materials-Seed/Slag Interactions and Effects, NBS Quarterly Progress Report to DOE, S. J. Schneider, December.

Plante, E. R. (1981). In, MHD Materials-Seed/Slag Interactions and Effects, NBS Quarterly Progress Report to DOE, S. J. Schneider, March.

Plante, E. R., Olson, C. D., and Negas, T. (1981). "Vapor Pressure Studies of K_2SO_4", to be published.

Plante, E. R., and Cook, L. P. (1978). 17th Symposium on Engineering Aspects of Magnetohydrodynamics, Stanford, CA. paper C.1.

Plante, E. R., Olson, C. D., and Negas, T. (1975). 6th International Conference on Magnetohydrodynamic Electrical Power Generation, II. p 211, Washington, DC.

Pressley, H. (1970). Trans. Brit. Ceram. Soc. 69, 205.

Preston, E. and Turner, W. E. S. (1933). J. Soc. Glass Tech., 17, 122.

Rapp, R. ed. (1981). International Conference on High Temperature Corrosion, San Diego, CA, March 2-6, NACE. Proceedings in press.

Raymon, N. S., and Sadler III, L. Y. (1976). "Refractory Lining Materials for Coal Gasifiers--A literature Review of Reactions Involving High-Temperature Gas and Alkali Metal Vapors", Information Circular, 8721. Bureau of Mines.

Rigby, G. R., and Hutton, R. (1962). J. Am. Ceram. Soc. 45, 68.

Sanders, D. M. and Haller, W. K. (1977). J. Amer. Ceram. Soc., 60, 3.

Sanders, D. M. and Haller, W. K. (1979). "A High Temperature Transpiration Apparatus for the Study of the Atmosphere Above Viscous Incongruently Vaporizing Melts." p. 111, ibid, Bonnell and Hastie.

Sanders, D. M., Blackburn, D. H., and Haller, W. K. (1976). J. Am. Ceram. Soc., 59, 366.

Sarofim, A. F., Howard, J. B., and Padia, A. S. (1977). Comb. Sci. Tech. 16, 187.

Sasaki, Y., and Belton, G. R. (1980). Met. Trans. 11B, 221.

Schneider, S. J., Frederikse, H. P. R., and Negas, T. (1980). "Materials for Open Cycle MHD Generators", Current Topics in Materials Science, 4, p 89.

Schwerdtfeger, K., and Schubert, H. G. (1978). Met. Trans. 9 B, 143.

Self, S. A. (1979). "Diagnostic Techniques in Combustion MHD Flows", ibid Bonnell and Hastie.

Shearer, J. A., Johnson, I., and Turner, C. B. (1979). Env. Sci. Tech. 13, 1113.

Spacil, H. S., and Luthra, K. L. (1979). J. Electrochem. Soc. 126, C134.

Spacil, H. S. and Luthra, K. L. (1980). "Thermochemistry of a Pressurized Fluidized Bed Coal Combustor/Gas Turbine Combined Cycle". GE Report 80CRD238. See also, CFCC Development Program (1978).

Staehle, R. W., ed. (1974). "Materials Problems and Research Opportunities in Coal Conversion", PB-248 081 (NTIS).

Stewart, G. W., Chakrabarti, A., Stinespring, C., and Castleton, K. (1980). "Deposition of Alkali in Coal Combustion Streams:, presented at the Fall Meeting, Western States Section, Comb. Inst., Los Angeles, CA (October).

Stwalley, W. C., and Koch, M. E. (1980). Opt. Eng. 19, 71.

Turkdogan, E. T. (1980). "Physical Chemistry of High Temperature Technology", Academic Press, New York, NY.

Venable, C. R., Jr. (1969). Am. Ceram. Soc. Bull., 48, 1114.

Vorres, K. S. (1980). Energy Res. 4, 109.

Wilson, J. S., and Redifer, M. W. (1974). Trans. ASME, J. Eng. Power A, 145.

Yannopoulos, L. N., Toth, J. L., and Pebler, A. (1977). Combust. Flame, 30, 61.

15. Figure Captions

1. Transpiration reactor showing internal details.

2. Partial pressure mass effusion data for molecular K_2SO_4 over $K_2SO_4(\ell)$ (Plante et al., 1981).
Open cirlces--present study, open triangles--Lau et al. (1979), closed triangles--Efimova and Gorokhov (1979).

3. Partial pressure data for KOH and $(KOH)_2$ over liquid KOH, obtained by TMS. Curves labelled Gusarov refer to data of Gusarov and Gorokhov (1968). JANAF curves are from JANAF (1971).

4. Partial pressure data for K, O_2, and SiO over illite. The triangular points were obtained by the TMS method with a N_2 atmosphere, all other data were obtained by KMS under vacuum vaporization conditions. The closed symbols refer to O_2 with ticks indicating increasing (up) or decreasing (down) temperature chronology.

5. Comparison of glass melt Na partial pressure data obtained by various workers (see text) for compositions (wt.%) similar to Na_2O(17), CaO(12), and SiO_2(71). KMS(1), 17.0 to 16.7 and KMS(3), 15.6 to 13.3 wt.%. TMS(1), 17.0 and TMS(2), 16.9 wt.%.

6. Activity coefficient data (TMS) for Na_2CO_3 (0.45 wt.%) in glass (see caption 5 for glass composition). Open circles and squares refer to run-chronology of increasing and decreasing temperature, respectively.

7. Non-equilibrium vaporization effect in the K_2O-Al_2O_3-SiO_2 system. Broken curve represents the pure $KAlSiO_4$ phase. Run chronology for the partially decomposed $KAlSiO_4$ system follows the temperature sequence ABC (KMS data).

8. Selected potassium partial pressure data (KMS data) for synthetic "Western" (W) and "Eastern" (E) MHD-channel slags with K_2O compositions (wt.%) of W_2 (19 to 17.6), W_3 (12.9 to 10.8) and E (23.3 to 22.1). "Eastern" slag data points omitted for clarity, but they are of similar precision to the "Western" slag data (see Plante and Cook, 1978).

9. Selected potassium and oxygen partial pressure data (KMS) for a synthetic "Eastern" MHD-channel slag with composition (K_2O wt.%) 23.3 to 22.8 (AB interval) and 22.8 to 22.1 (BC interval). Run chronology follows the temperature sequence ABC. Open and closed circles (and solid curves) refer to potassium data, with increasing and decreasing temperature run-chronology, respectively. Open and closed triangles (and dashed curves) refer to oxygen data, with increasing and decreasing temperature run-chronology, respectively.

10. Partial pressure variation of initial volatiles (K_2O, 19.5 to 19.1 wt.%) as a function of temperature (and time) for the K_1 slag (liquidus temperature $\sim$ 1700 $\pm$ 30 K) using the TMS approach (run 1). Conditions: 0.5 atm N_2, capillary probe. Dashed comparison curves represent K-pressures over the K_2CO_3 and $KAlO_2$ phases.

11. KMS data for variation of K_2O activity coefficient with temperature and composition for the K_1 slag. The numbers, ranging from 0.154 to 0.08, refer to the mole fraction of K_2O remaining in the sample at each measurement point. Runs 1 to 3 were carried out consecutively on the same sample. The open square data point at 1575 K, run 1, was obtained by TMS with additional O_2 present.

12. Vaporization of K and O_2 from the K_2 slag. Open circles--O_2 (KMS), closed circles--O_2 (TMS), open triangles--K (KMS), closed triangles--K (TMS). Chronological order of data taken with increasing temperature except for ticked data points where the temperature was decreasing.

13. Typical K^+ ion intensity signal-decay with time for K_2 slag. TMS conditions: temperature, 1570 K; N_2 carrier gas pressure, 0.21 atm; capillary nozzle.

14. Comparison of K_2O dissociation pressure-product data for the MHD plasma with 1 wt.% K_2CO_3 seed (broken curves) and slag (solid curves) phases. Curve A is for the actual slag (K_1) with 14 wt.% K_2O content, B is for the Synthetic "Western" slag with 18 wt.% K_2O, and C is for the quarternary Simplified "Western" slag with 15 wt.% K_2O.

15. Thermodynamic activities (TMS data) for NaCl and KCl in the K_1 slag-alkali exchange process. The indicated reference state partial pressures were obtained from JANAF (1971).

16. Silica activity function (KMS data). K_p refers to the reaction, $SiO_2(c) + H_2 = SiO + H_2O$. Open circles are for illite and closed circles represent similar data obtained using quartz but with a much larger sample surface area. Dashed curve represents JANAF (1971) data for unit activity silica.

17. Equilibrium constant for H_2O dissociation (KMS data). Open circles, data obtained during illite + H_2 experiment; open squares, H_2O rather than H_2 addition; closed circles, P_{H_2} assumed equal to $2P_{O_2}$ for K_p calculation. Dashed curve, JANAF (1971) data.

18. Variation of K-pressure (open symbols) and O_2-pressure (closed symbols) with H_2O-pressure for K_2 slag in the presence of added H_2. TMS conditions: temperature, 1655 K; N_2 carrier gas pressure, 0.18 atm; capillary nozzle. Arrows indicate run chronology.

19. Isothermal (1610 K) dependence of K-pressure on H_2O-pressure for the K_2 slag with added H_2O. TMS conditions: N_2 carrier gas pressure, 0.21 atm; capillary nozzle.

20. Isothermal dependence of KOH-pressure on H_2O apparent pressure for the K_2 slag at 1794 K. KMS data with Pt-cell orifice diameter of 0.34 mm. The curve of slope 0.5 represents the theoretical pressure dependence for reaction [10] (see text).

21. Computer-calculated distribution of alkali-containing vapor species as a function of temperature for the non-ideal solution glass-combustion gas system specified in table 3.

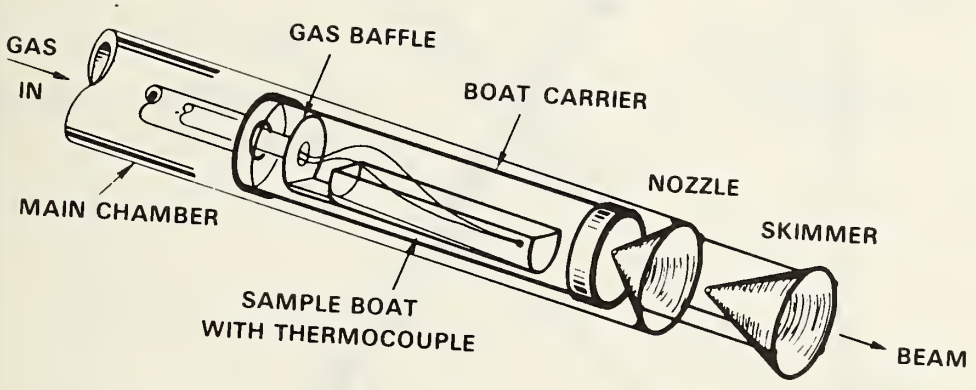
GAS
IN
GAS BAFFLE
BOAT CARRIER
NOZZLE
SKIMMER
MAIN CHAMBER
SAMPLE BOAT
WITH THERMOCOUPLE
BEAM

Figure 1

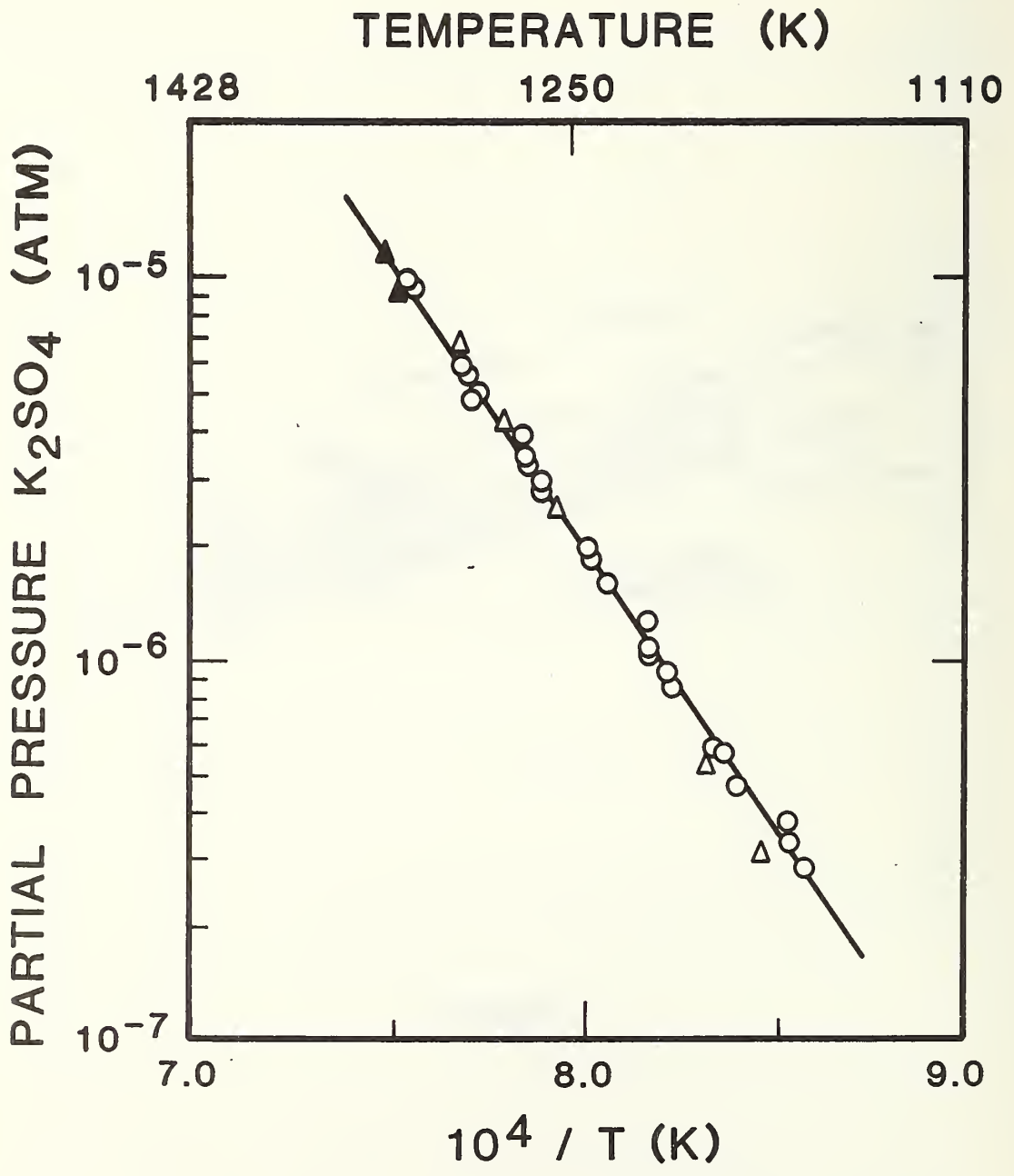
TEMPERATURE (K)
1428
1250
1110
PARTIAL PRESSURE K_2SO_4 (ATM)
10^{-5}
10^{-6}
10^{-7}
7.0
8.0
9.0
10^4 / T (K)

Figure 2

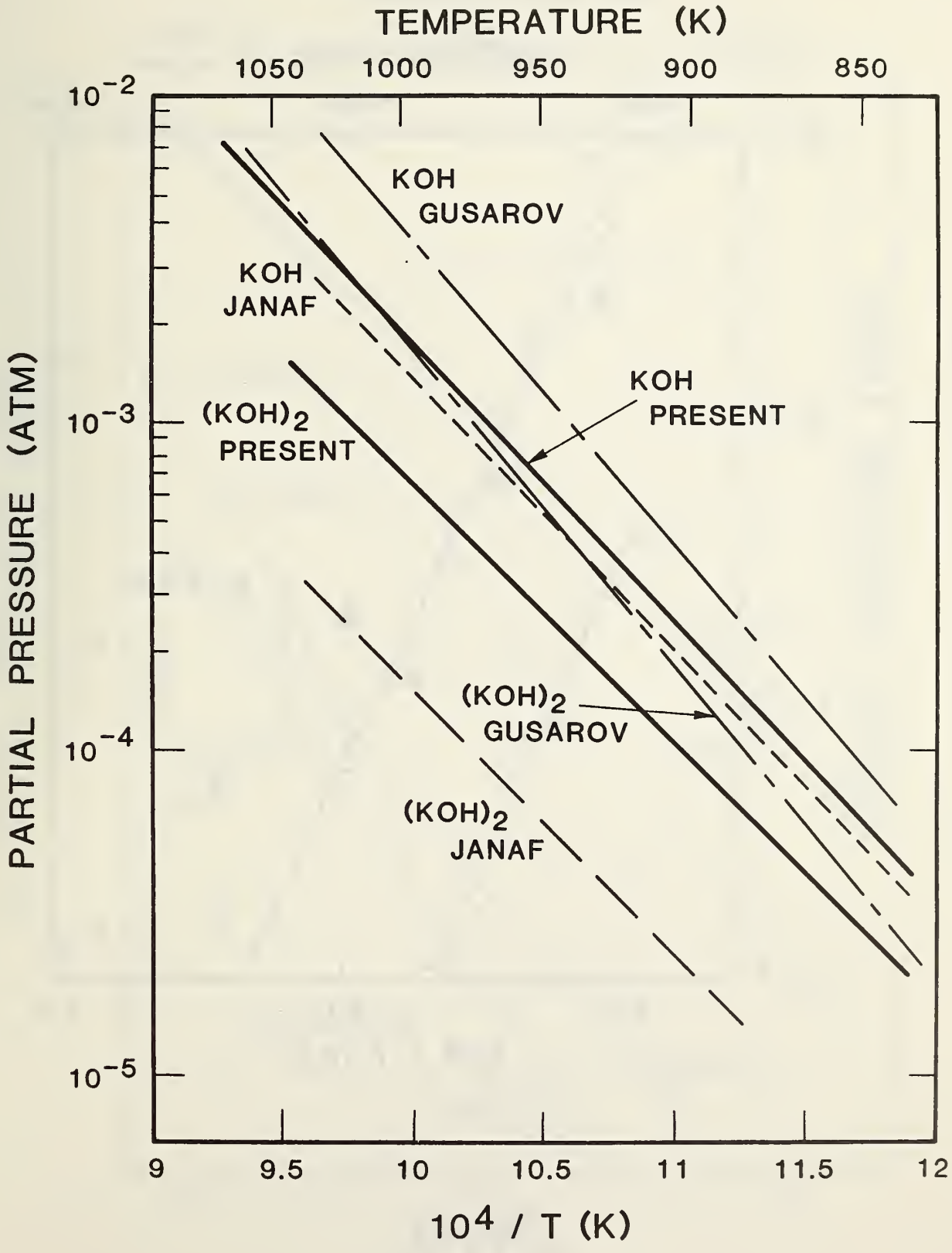
TEMPERATURE (K)
1050
1000
950
900
850
10^{-2}
10^{-3}
10^{-4}
10^{-5}
PARTIAL PRESSURE (ATM)
KOH
GUSAROV
KOH
JANAF
KOH
PRESENT
$(KOH)_2$
PRESENT
$(KOH)_2$
GUSAROV
$(KOH)_2$
JANAF
9
9.5
10
10.5
11
11.5
12
10^4 / T (K)

Figure 3

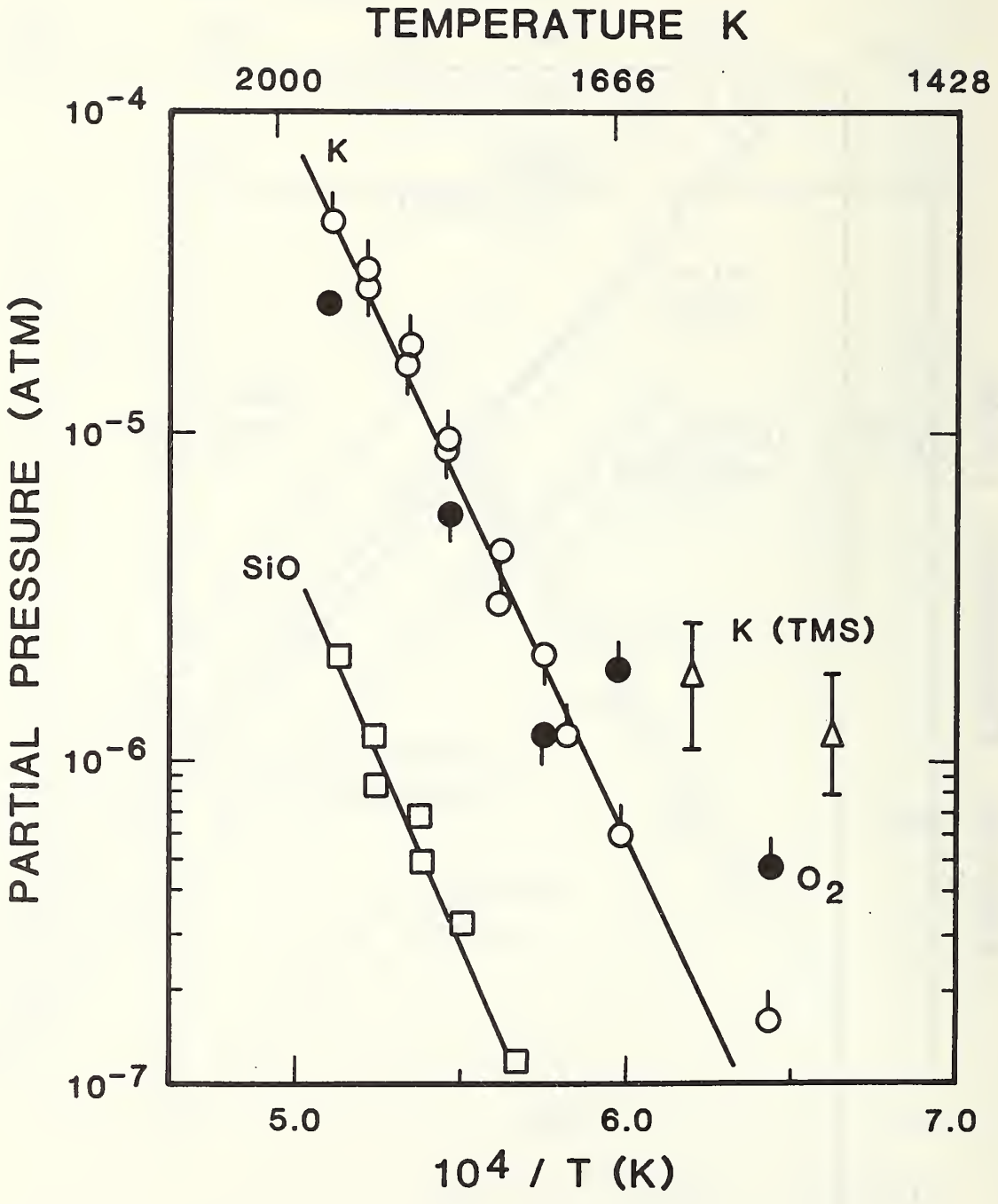
TEMPERATURE K
2000
1666
1428
10^{-4}
10^{-5}
10^{-6}
10^{-7}
PARTIAL PRESSURE (ATM)
K
SiO
K (TMS)
O_2
5.0
6.0
7.0
10^4 / T (K)

Figure 4

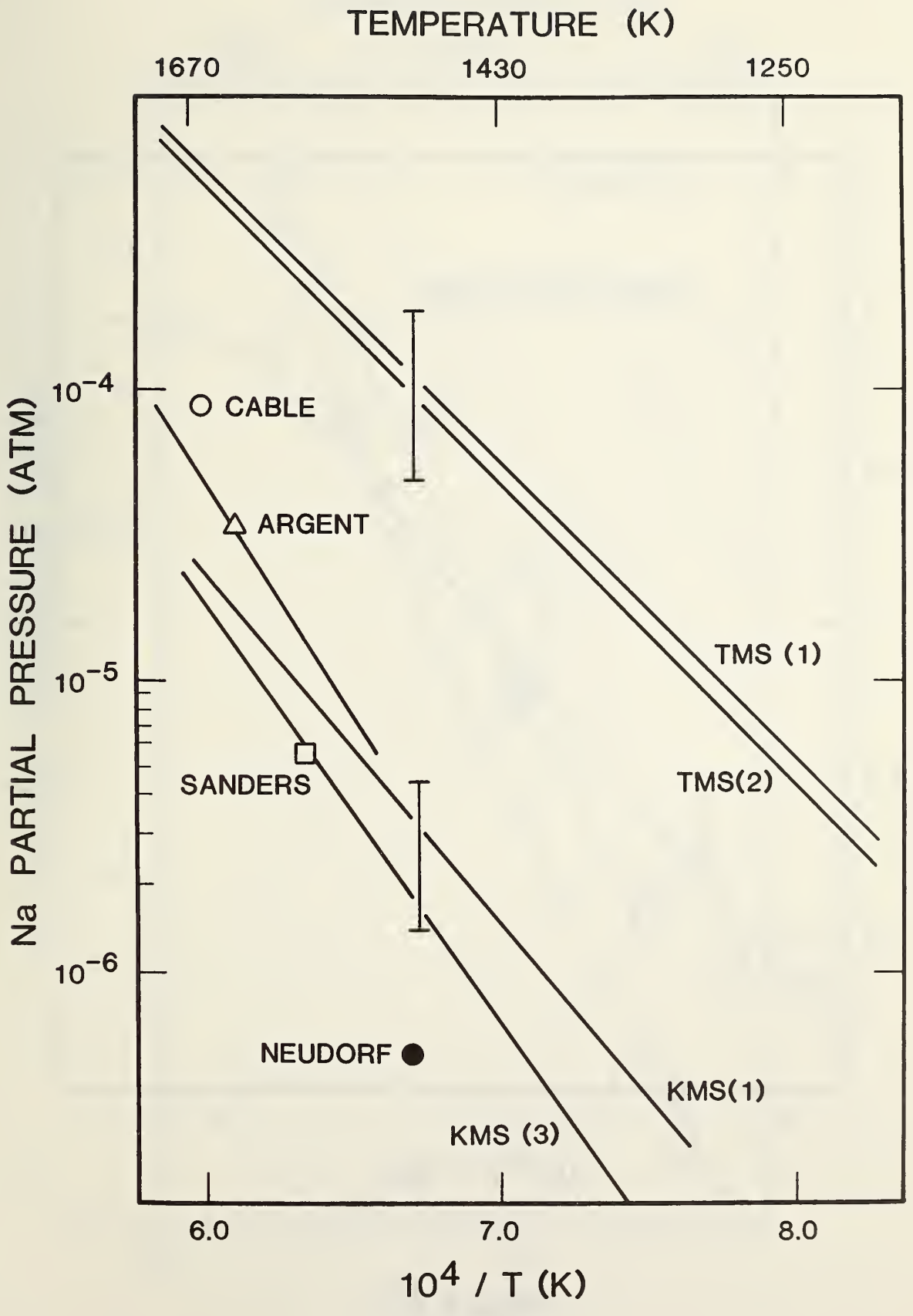
TEMPERATURE (K)
1670
1430
1250
Na PARTIAL PRESSURE (ATM)
10^{-4}
10^{-5}
10^{-6}
CABLE
ARGENT
SANDERS
NEUDORF
TMS (1)
TMS(2)
KMS(1)
KMS (3)
6.0
7.0
8.0
10^4 / T (K)

Figure 5

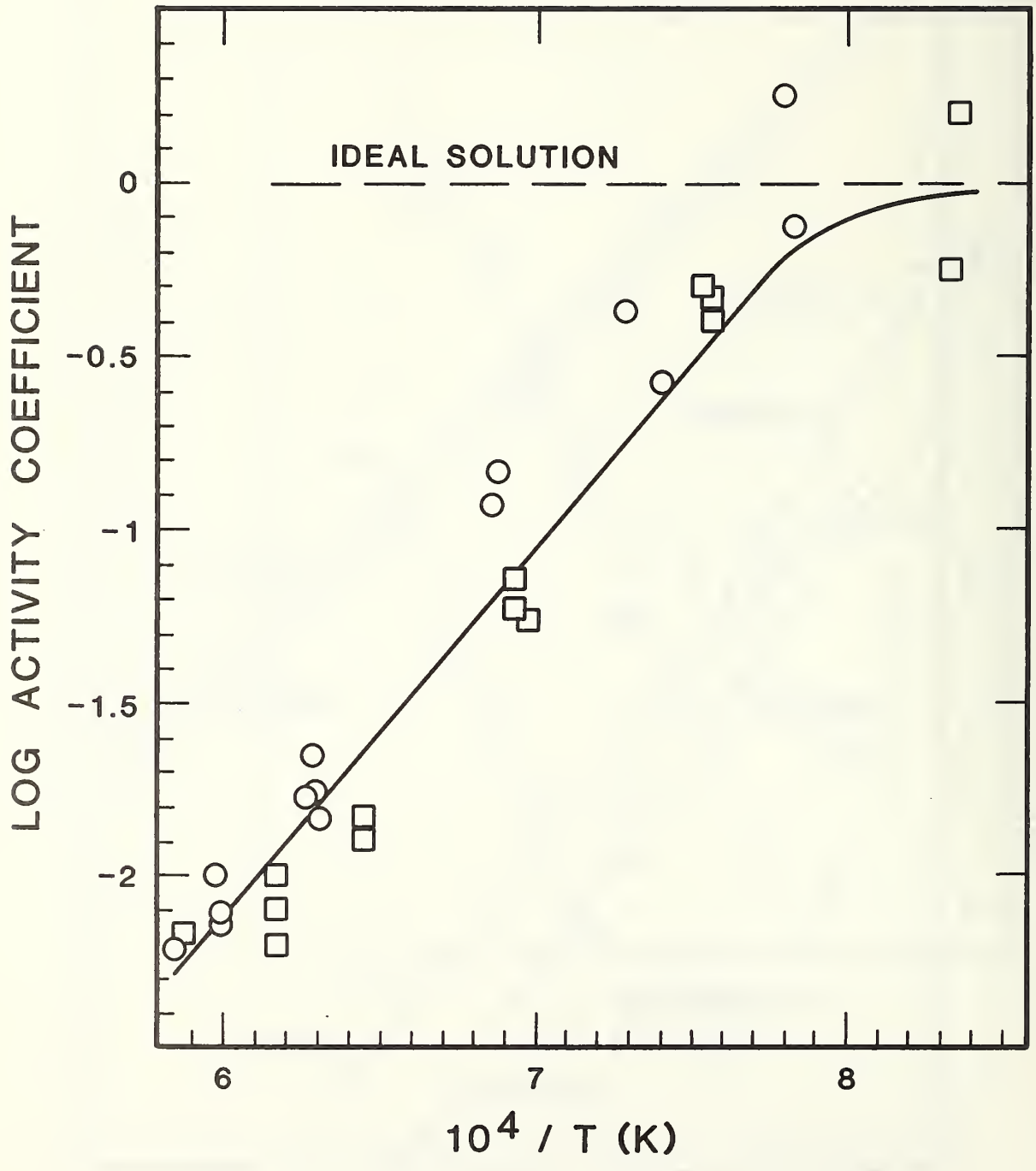
IDEAL SOLUTION
LOG ACTIVITY COEFFICIENT
0
-0.5
-1
-1.5
-2
6
7
8
10^4 / T (K)

Figure 6

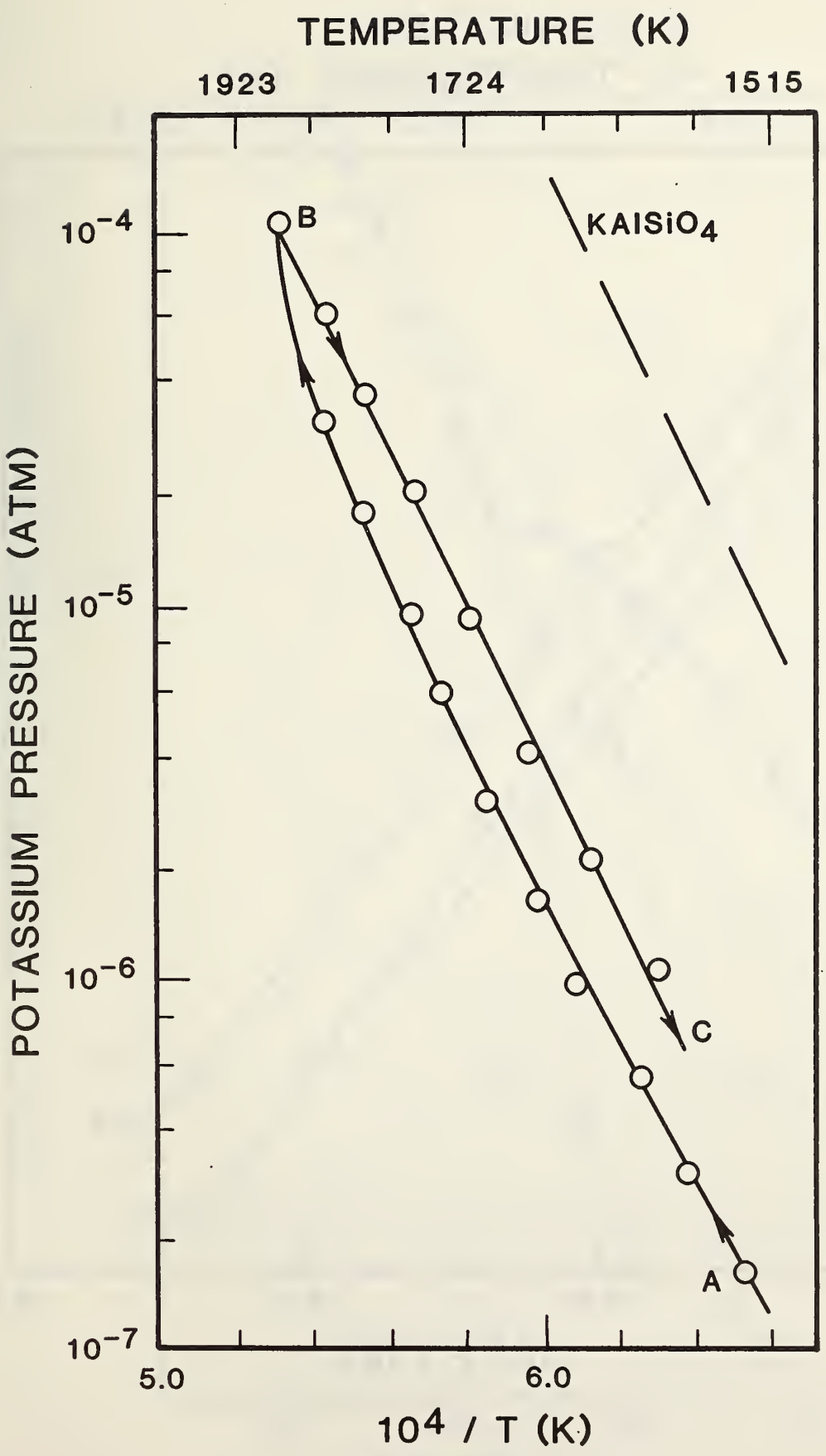
TEMPERATURE (K)
1923
1724
1515
10^{-4}
10^{-5}
10^{-6}
10^{-7}
POTASSIUM PRESSURE (ATM)
B
C
A
$KAlSiO_4$
5.0
6.0
10^4 / T (K)

Figure 7

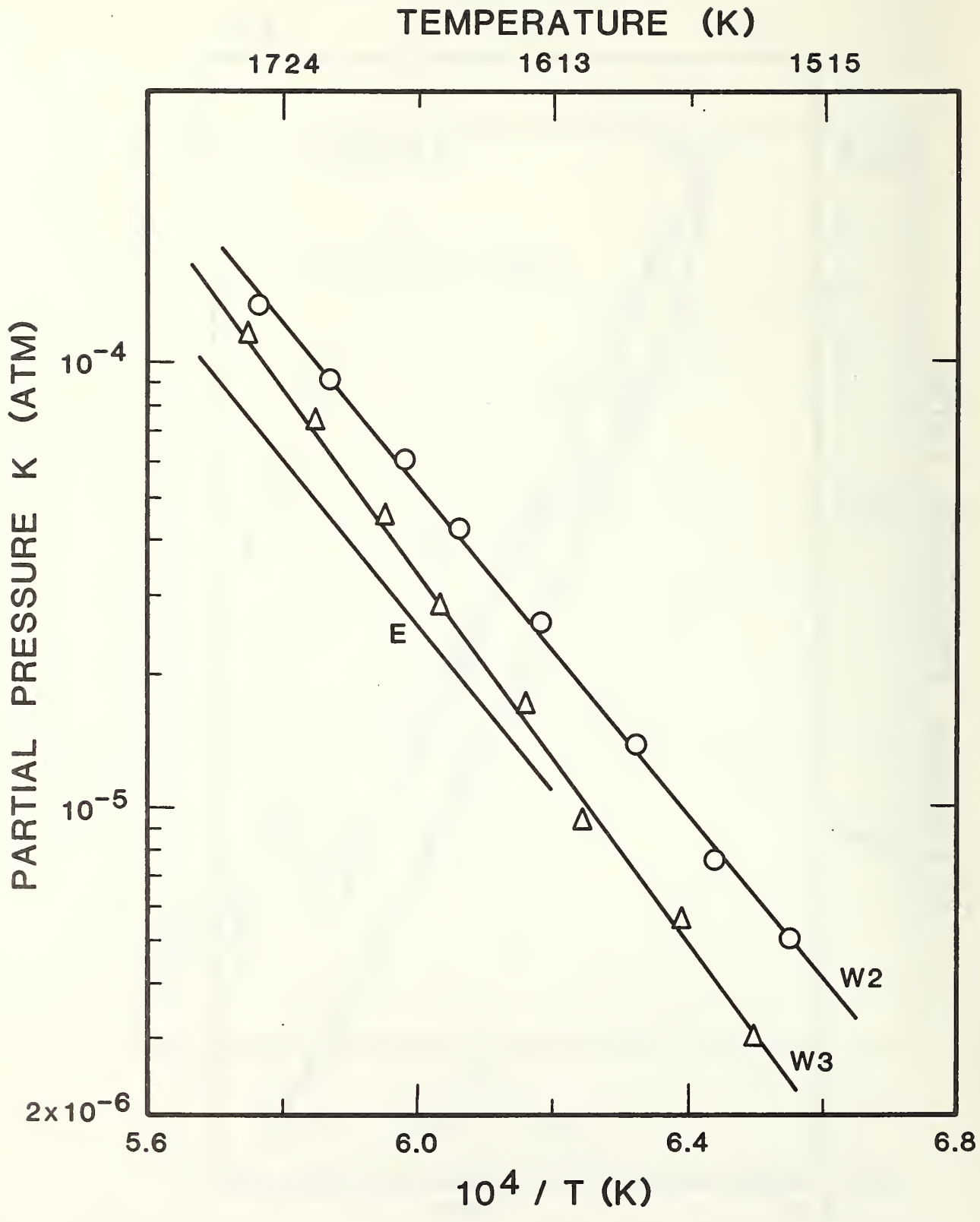
TEMPERATURE (K)
1724
1613
1515
PARTIAL PRESSURE K (ATM)
10^{-4}
10^{-5}
2×10^{-6}
E
W2
W3
5.6
6.0
6.4
6.8
10^4 / T (K)

Figure 8

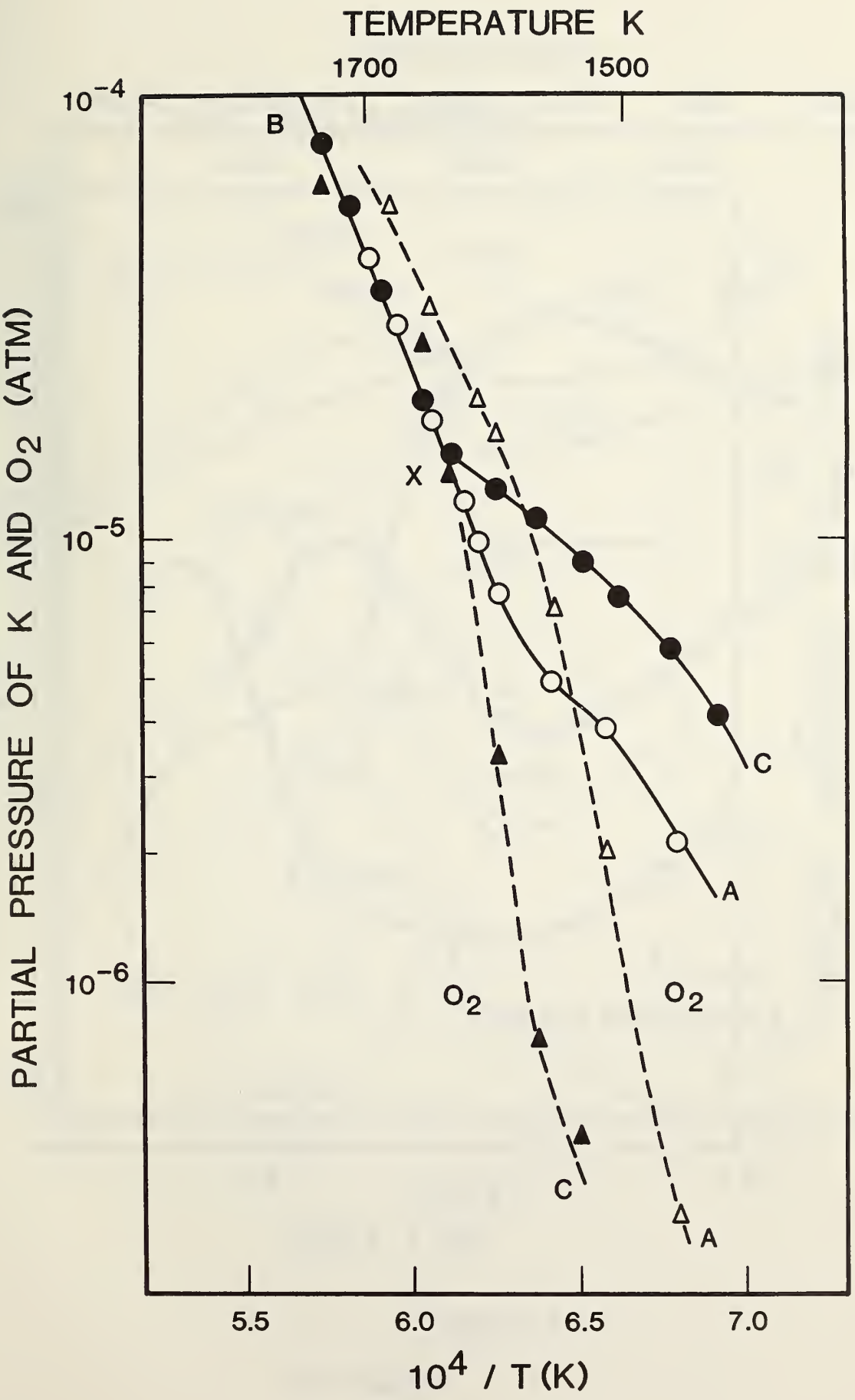
TEMPERATURE K
1700
1500
10^{-4}
10^{-5}
10^{-6}
PARTIAL PRESSURE OF K AND O_2 (ATM)
B
X
C
A
O_2
O_2
C
A
5.5
6.0
6.5
7.0
10^4 / T (K)

Figure 9

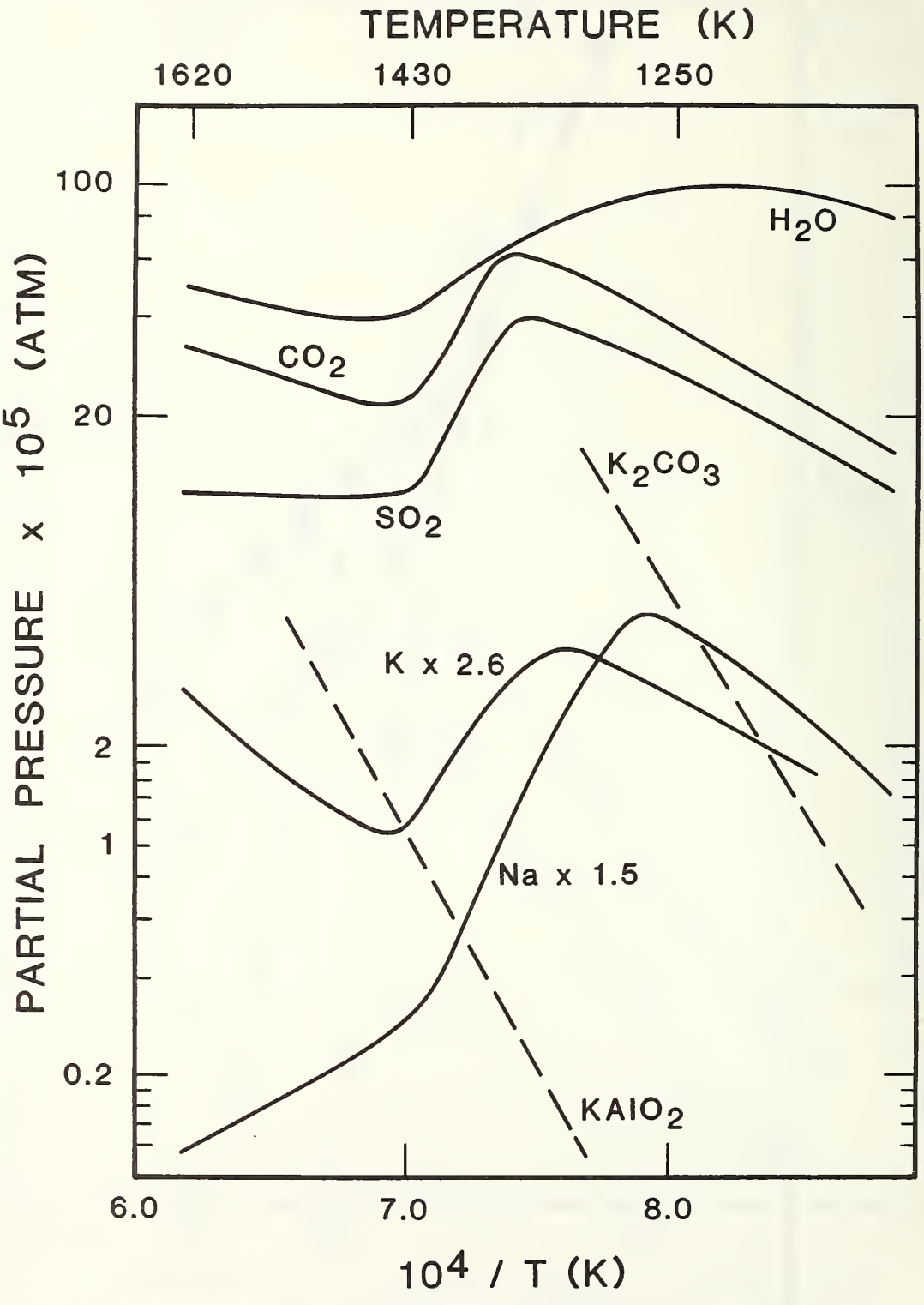
TEMPERATURE (K)
1620
1430
1250
100
20
2
1
0.2
PARTIAL PRESSURE x 10^5 (ATM)
H_2O
CO_2
SO_2
K_2CO_3
K x 2.6
Na x 1.5
$KAlO_2$
6.0
7.0
8.0
10^4 / T (K)

Figure 10

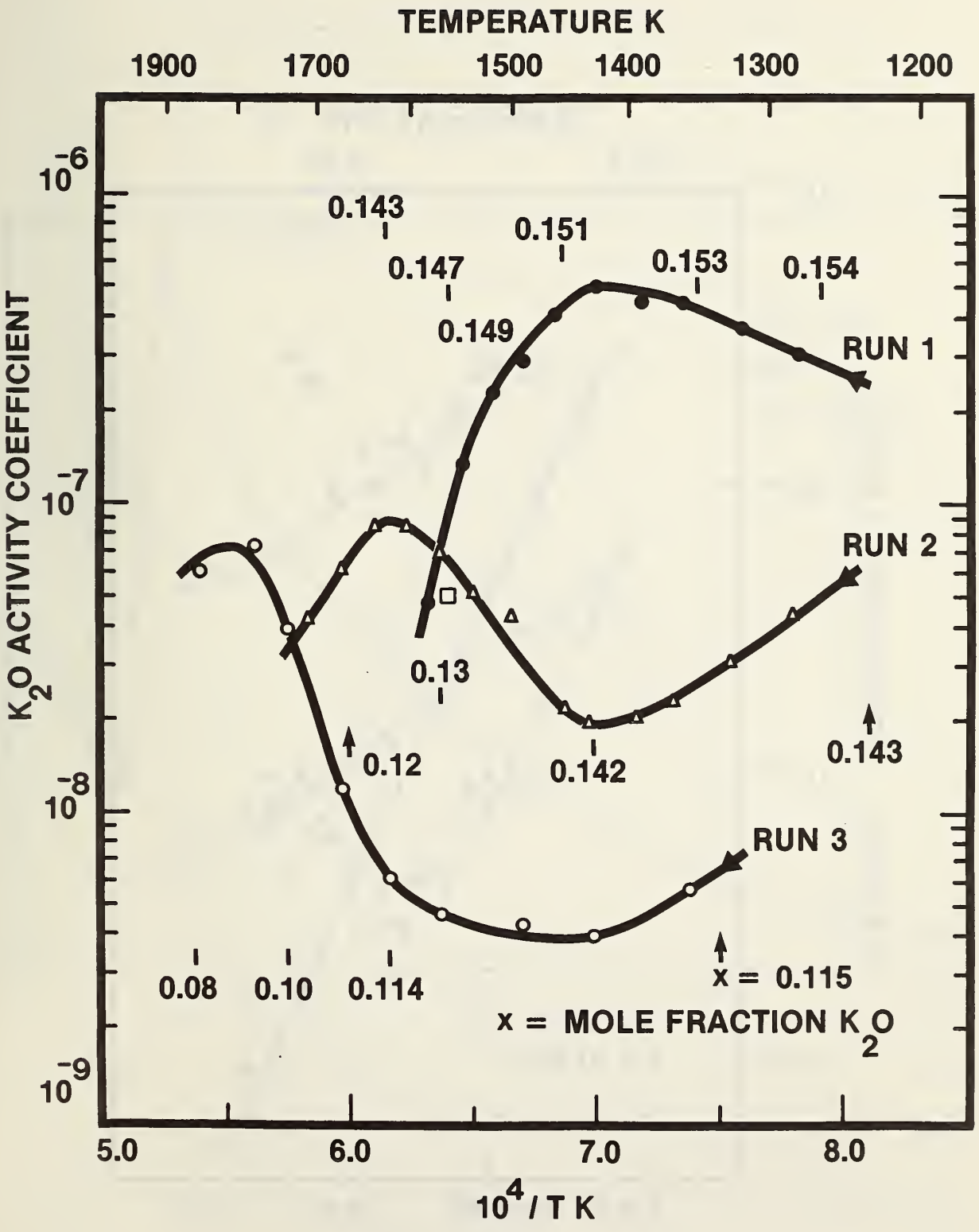
TEMPERATURE K
1900
1700
1500
1400
1300
1200
10^{-6}
10^{-7}
10^{-8}
10^{-9}
K_2O ACTIVITY COEFFICIENT
0.143
0.147
0.149
0.151
0.153
0.154
RUN 1
RUN 2
RUN 3
0.13
0.12
0.142
0.143
0.08
0.10
0.114
x = 0.115
x = MOLE FRACTION K_2O
5.0
6.0
7.0
8.0
10^4 / T K

Figure 11

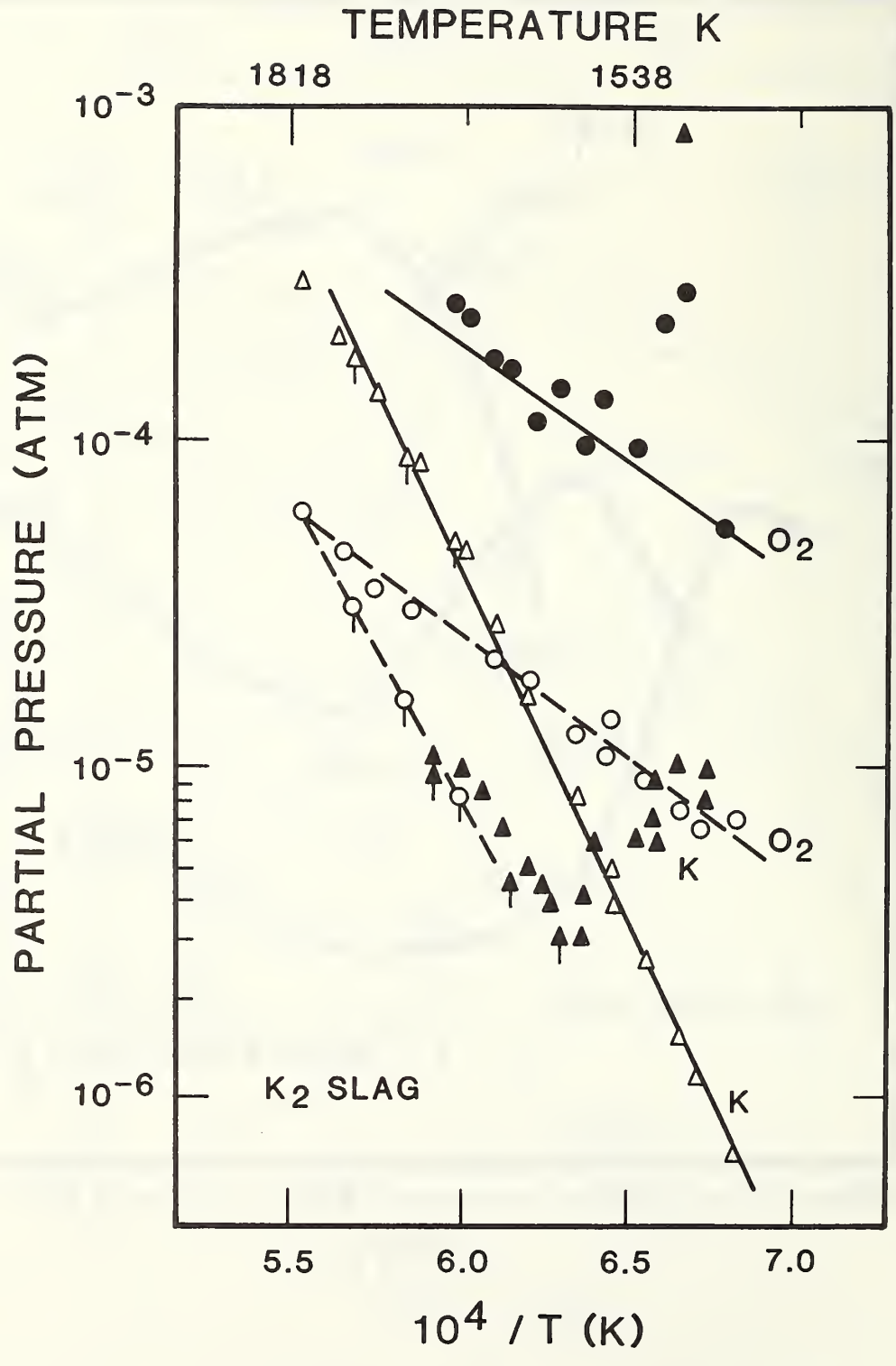
TEMPERATURE K
1818
1538
10^{-3}
10^{-4}
10^{-5}
10^{-6}
PARTIAL PRESSURE (ATM)
O_2
O_2
K
K
K_2 SLAG
5.5
6.0
6.5
7.0
10^4 / T (K)

Figure 12

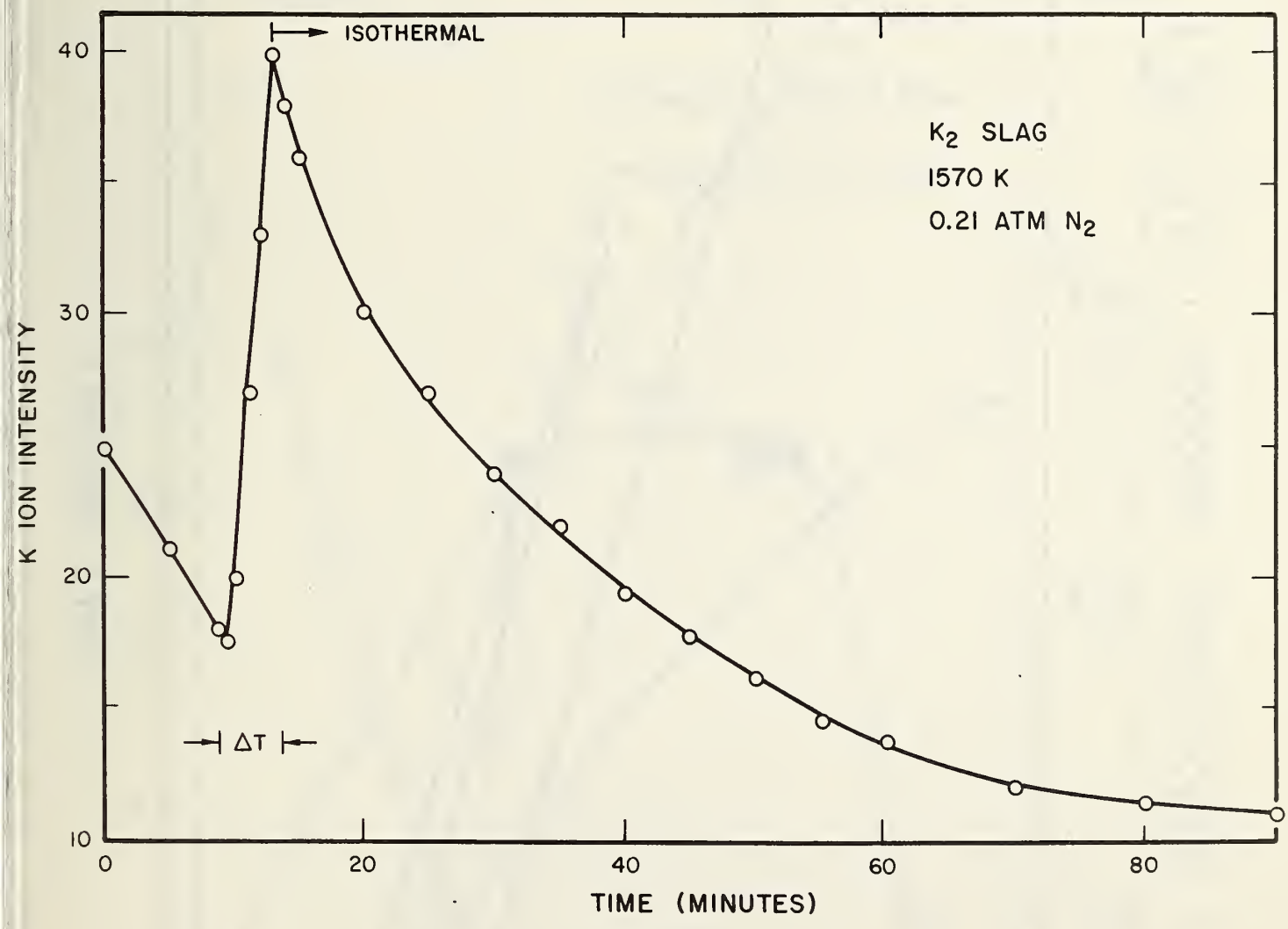
ISOTHERMAL
K_2 SLAG
1570 K
0.21 ATM N_2
ΔT
K ION INTENSITY
TIME (MINUTES)
40
30
20
10
0
20
40
60
80

Figure 13

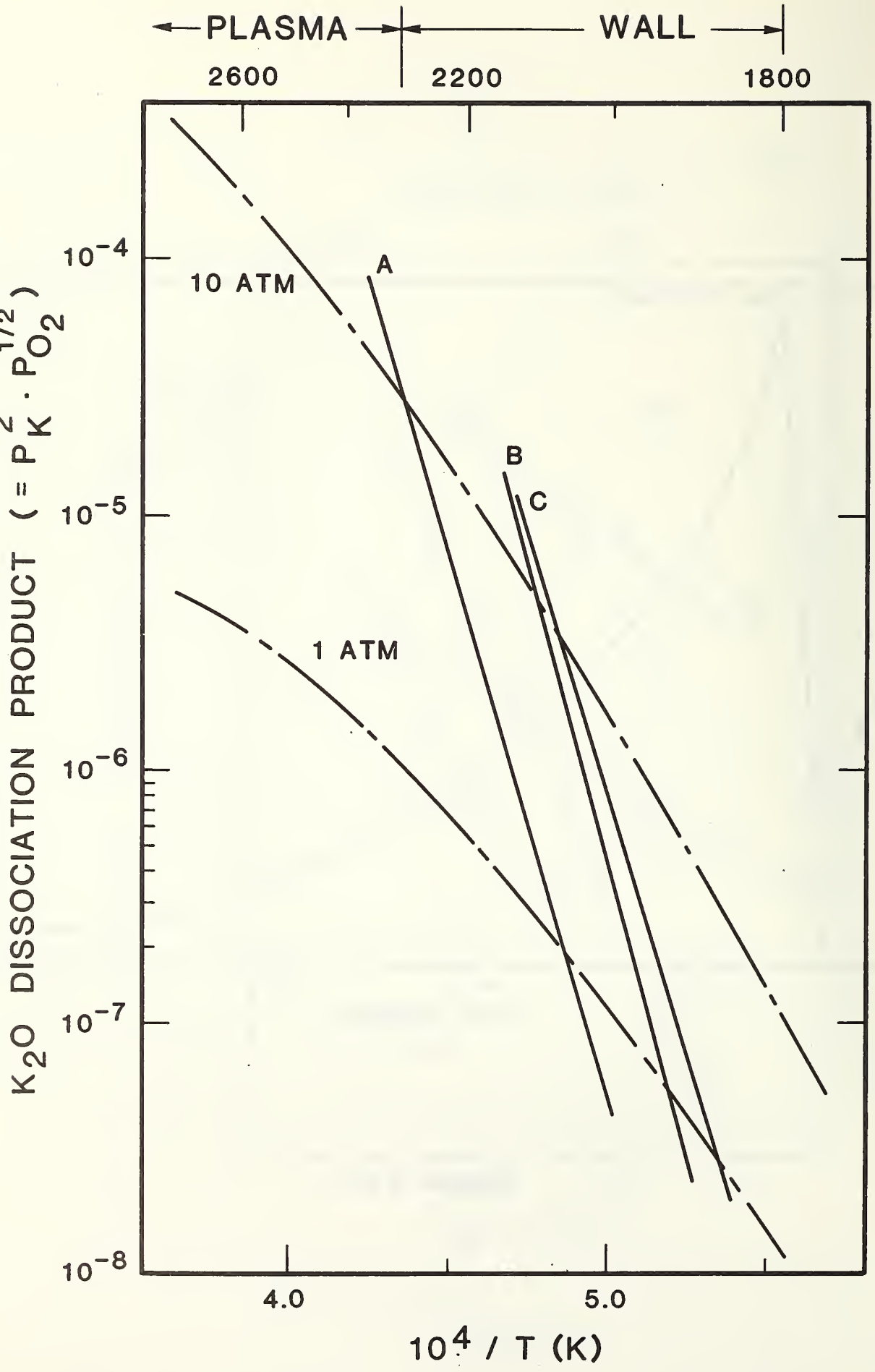
PLASMA
WALL
2600
2200
1800
10 ATM
1 ATM
A
B
C
10^{-4}
10^{-5}
10^{-6}
10^{-7}
10^{-8}
K_2O DISSOCIATION PRODUCT ($= P_K^2 \cdot P_{O_2}^{1/2}$)
4.0
5.0
10^4 / T (K)

Figure 14

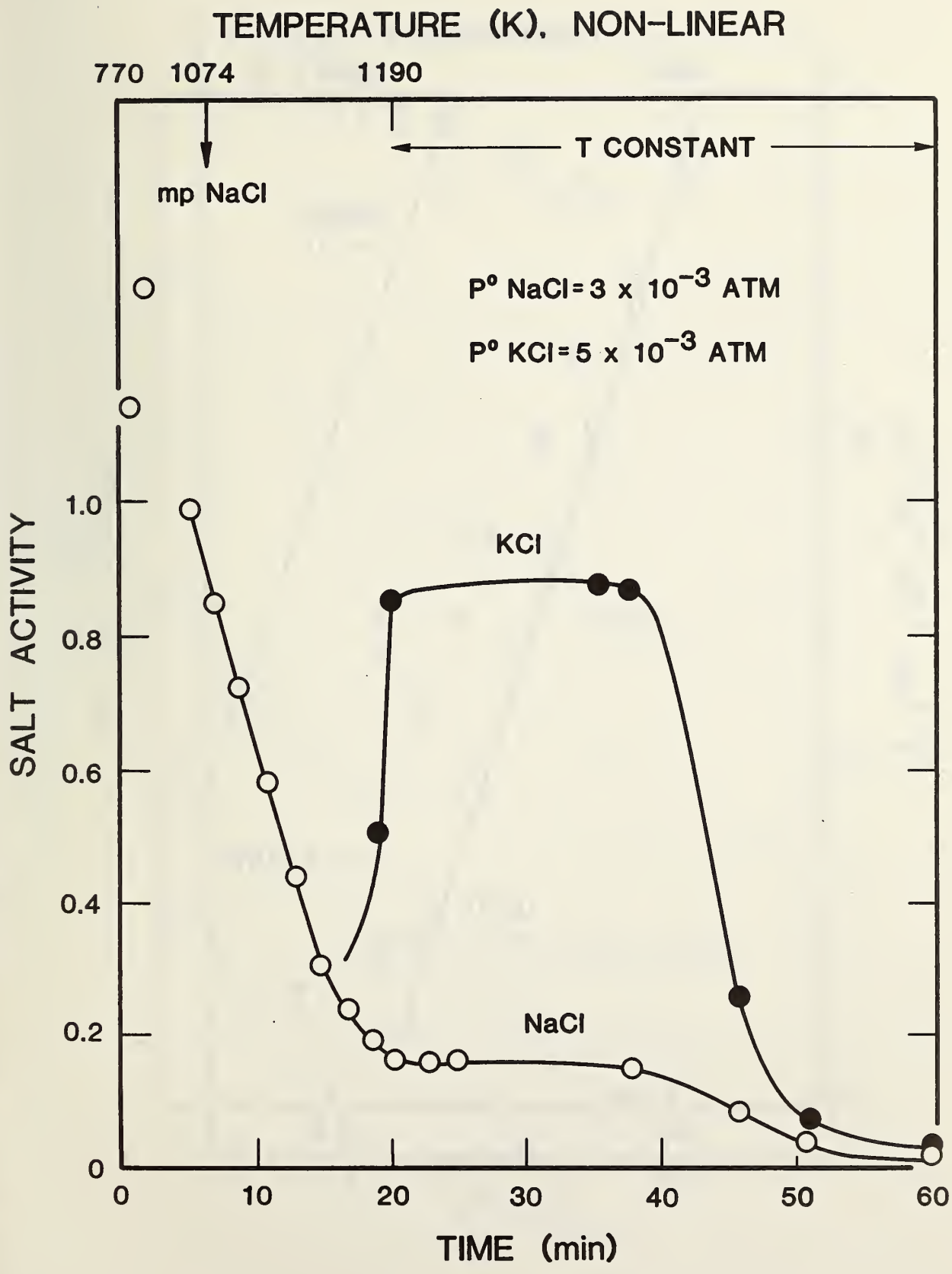
TEMPERATURE (K), NON-LINEAR
770
1074
1190
T CONSTANT
mp NaCl
P° NaCl = 3 x 10⁻³ ATM
P° KCl = 5 x 10⁻³ ATM
KCl
NaCl
SALT ACTIVITY
1.0
0.8
0.6
0.4
0.2
0
0
10
20
30
40
50
60
TIME (min)

Figure 15

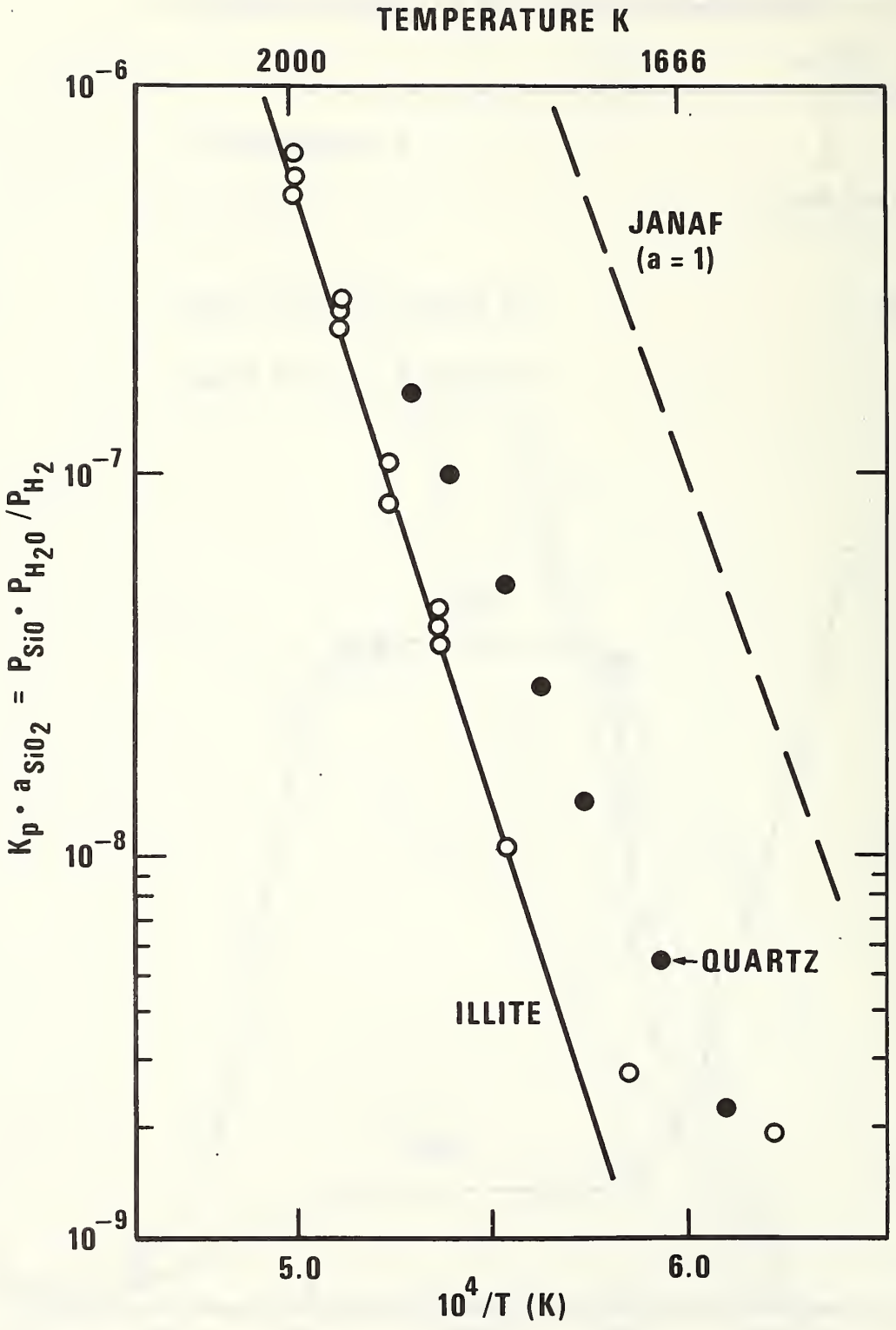
TEMPERATURE K
2000
1666
10^{-6}
10^{-7}
10^{-8}
10^{-9}
$K_p \cdot a_{SiO_2} = P_{SiO} \cdot P_{H_2O} / P_{H_2}$
JANAF
(a = 1)
QUARTZ
ILLITE
5.0
6.0
$10^4/T$ (K)

Figure 16

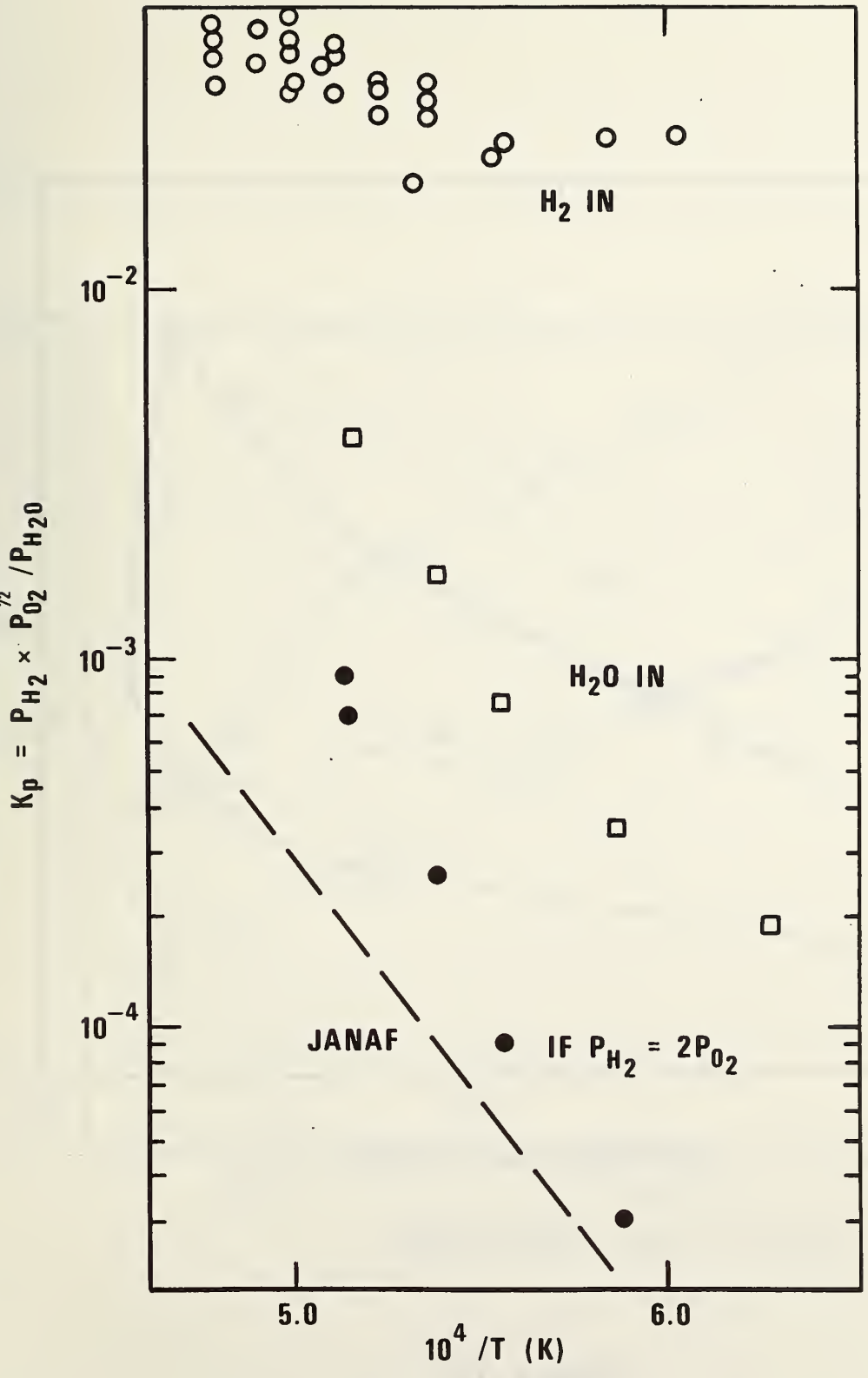
H_2 IN
H_2O IN
JANAF
IF $P_{H_2} = 2P_{O_2}$
10^{-2}
10^{-3}
10^{-4}
5.0
6.0
10^4 /T (K)
$K_p = P_{H_2} \times P_{O_2}^{1/2} / P_{H_2O}$

Figure 17

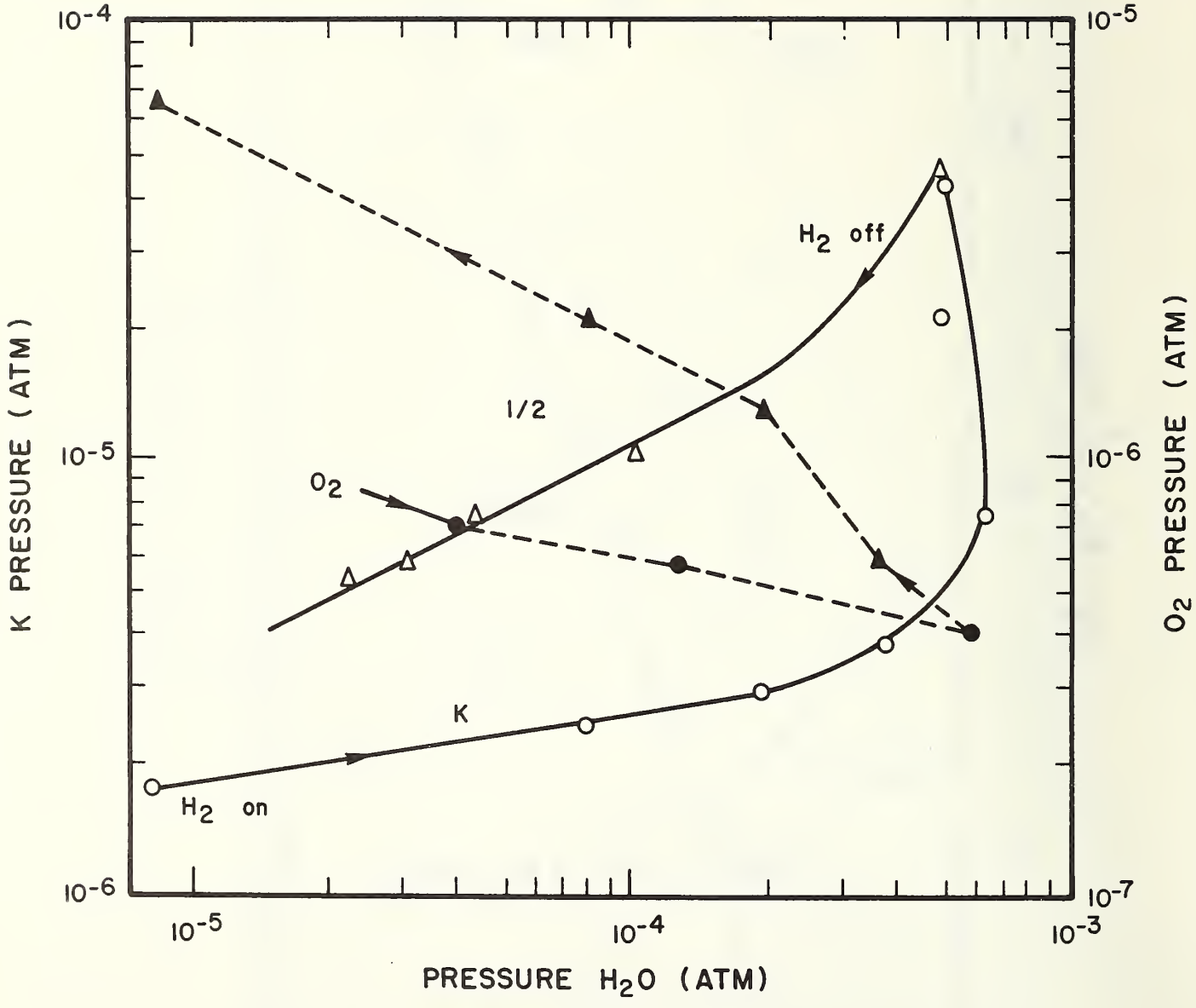
10-4
10-5
10-6
10-5
10-6
10-7
10-5
10-4
10-3
K PRESSURE (ATM)
O2 PRESSURE (ATM)
PRESSURE H2O (ATM)
H2 off
1/2
O2
K
H2 on

Figure 18

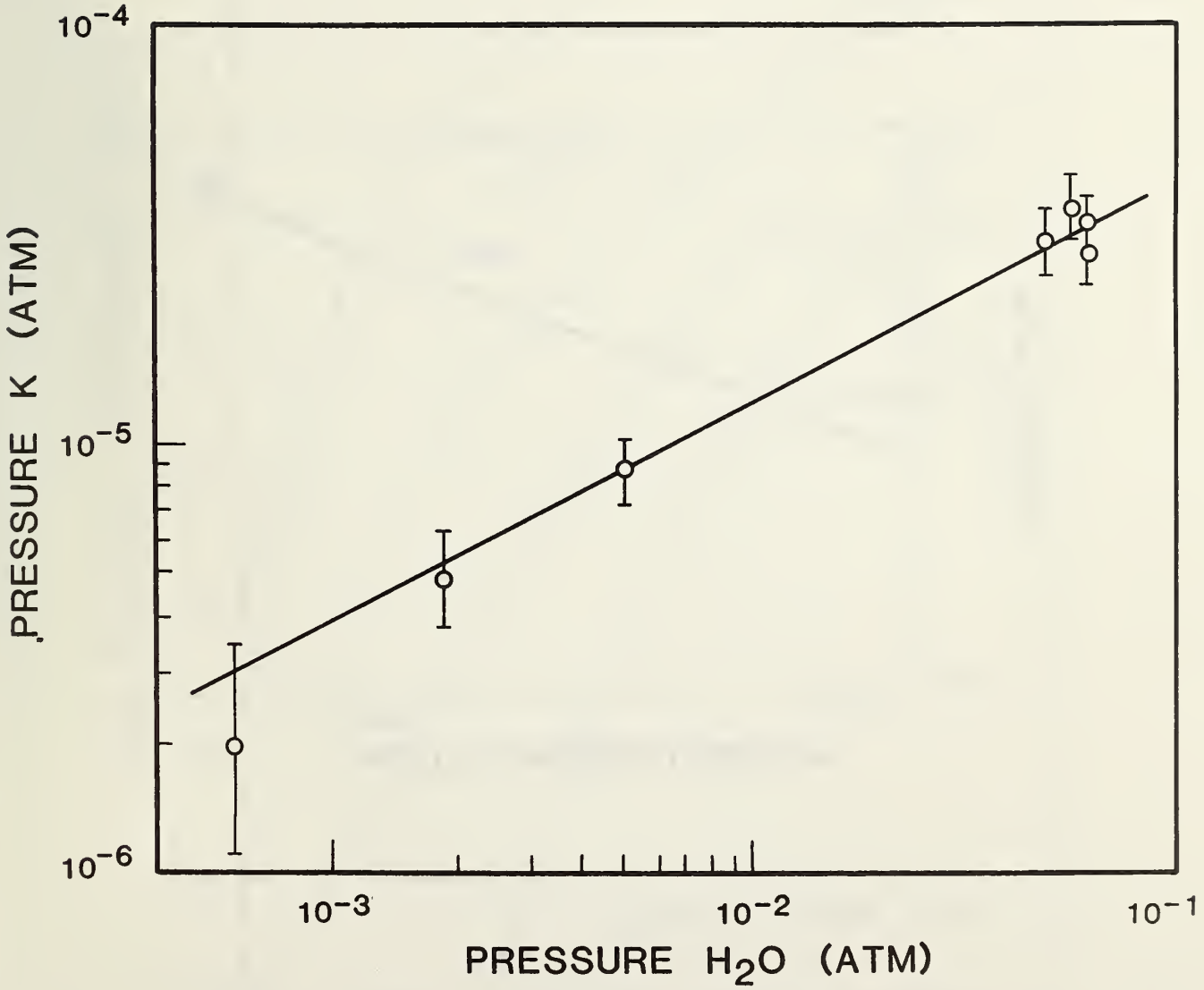

Figure 19

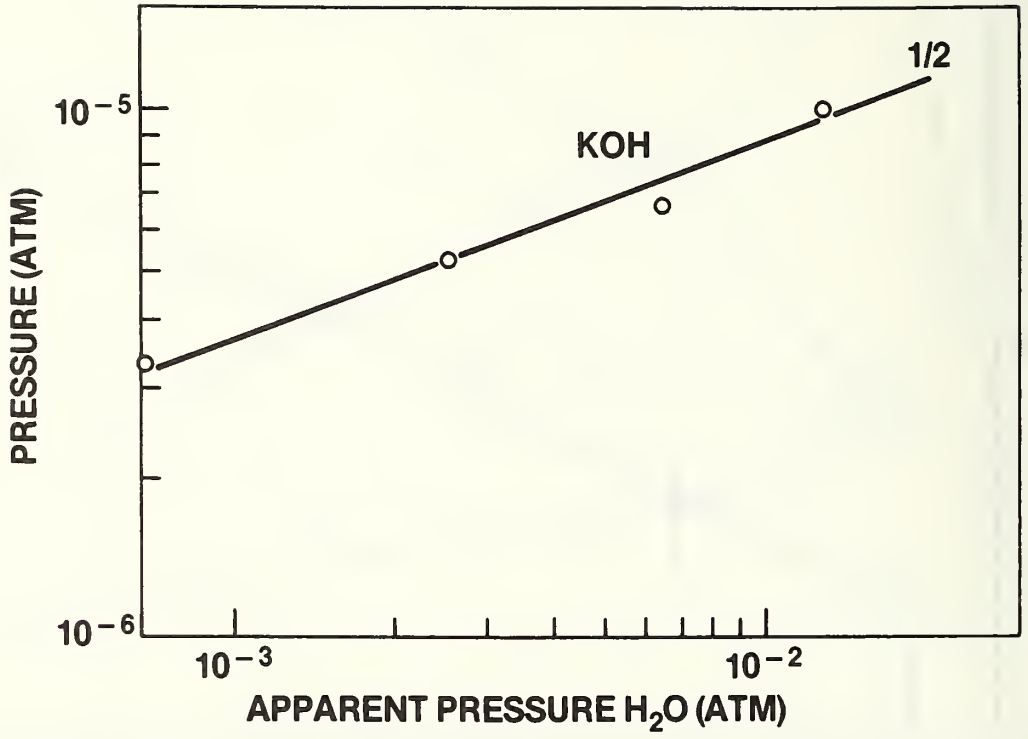
1/2
KOH
10^{-5}
10^{-6}
PRESSURE (ATM)
10^{-3}
10^{-2}
APPARENT PRESSURE H_2O (ATM)

Figure 20

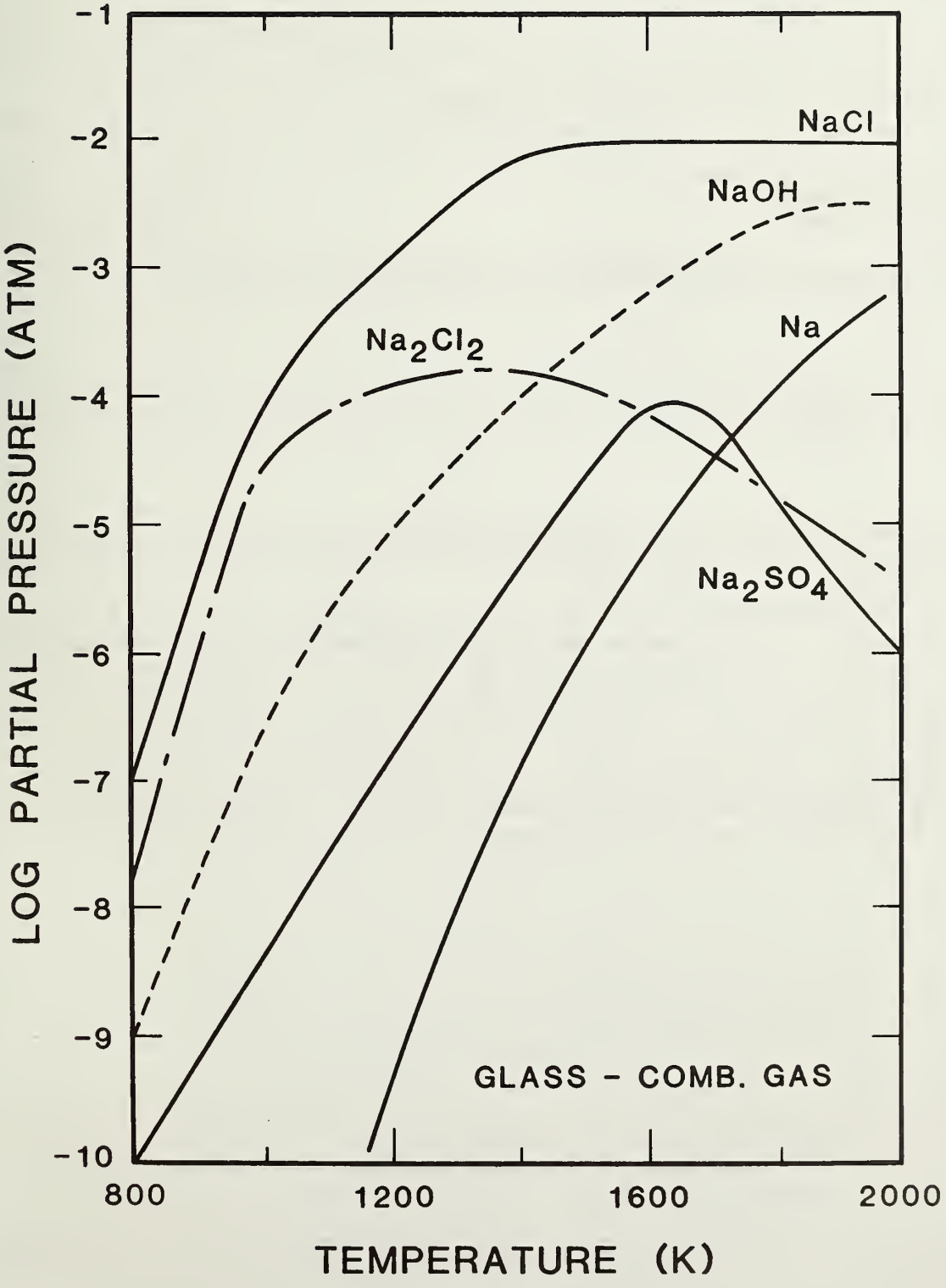
LOG PARTIAL PRESSURE (ATM)
-1
-2
-3
-4
-5
-6
-7
-8
-9
-10
NaCl
NaOH
Na_2Cl_2
Na
Na_2SO_4
GLASS - COMB. GAS
800
1200
1600
2000
TEMPERATURE (K)

Figure 21

NBS-114A (REV. 2-8C)

U.S. DEPT. OF COMM. BIBLIOGRAPHIC DATA SHEET (See instructions)	1. PUBLICATION OR REPORT NO.	2. Performing Organ. Report No.	3. Publication Date

4. TITLE AND SUBTITLE

Alkali Vapor Transport in Coal Conversion and Combustion Systems

5. AUTHOR(S)

J. W. Hastie, E. R. Plante, and D. W. Bonnell

6. PERFORMING ORGANIZATION (If joint or other than NBS, see instructions)

NATIONAL BUREAU OF STANDARDS
DEPARTMENT OF COMMERCE
WASHINGTON, D.C. 20234

7. Contract/Grant No.

8. Type of Report & Period Covered

Interim Report

9. SPONSORING ORGANIZATION NAME AND COMPLETE ADDRESS (Street, City, State, ZIP)

10. SUPPLEMENTARY NOTES

☐ Document describes a computer program; SF-185, FIPS Software Summary, is attached.

11. ABSTRACT (A 200-word or less factual summary of most significant information. If document includes a significant bibliography or literature survey, mention it here)

Alkali metal-containing vapor species are ubiquitous in coal conversion and combustion systems. These species originate from coal mineral and atmospheric impurities (organic and inorganic) and from ceramic construction materials. Alternatively, they are present as additives, such as with potassium seeding for MHD or with bulk glass as a particle absorbing medium, or with dolomite in fluidized bed systems. Alkali vapor transport over representative slag, glass, and simple halide, hydroxide, and sulfate systems is discussed in relation to materials and process limitations in coal-supported energy systems. Problems associated with molecular-level vapor transport measurements are also considered.

12. KEY WORDS (Six to twelve entries; alphabetical order, capitalize only proper names; and separate key words by semicolons)

13. AVAILABILITY

☒ Unlimited

☐ For Official Distribution. Do Not Release to NTIS

☐ Order From Superintendent of Documents, U.S. Government Printing Office, Washington, D.C. 20402.

☐ Order From National Technical Information Service (NTIS), Springfield, VA. 22161

14. NO. OF PRINTED PAGES

15. Price